www.sciencemag.org/content/356/6345/1362/suppl/DC1

Supplementary Materials for

Estimating economic damage from climate change in the United States

Solomon Hsiang,* Robert Kopp,* Amir Jina, James Rising, Michael Delgado, Shashank Mohan, D. J. Rasmussen, Robert Muir-Wood, Paul Wilson, Michael Oppenheimer, Kate Larsen, Trevor Houser

*Corresponding author. Email: shsiang@berkeley.edu (S.H.); robert.kopp@rutgers.edu (R.K.)

Published 30 June 2017, *Science* **356**, 1362 (2017)
DOI: 10.1126/science.aal4369

This PDF file includes:

Supplementary Materials

"Estimating Economic Damage in the United States from Climate Change"

Solomon Hsiang, Robert Kopp, Amir Jina, James Rising, Michael Delgado,

Shashank Mohan, D.J. Rasmussen, Robert Muir-Wood, Paul Wilson,

Michael Oppenheimer, Kate Larsen and Trevor Houser

Table of Contents

Authors' Note: This analysis builds on the technical analysis developed in our 2015 book "Economic Risks of Climate Change" (*41*) which in turn built on the proposed research program described in the 2013 conference paper "Empirically calibrating damage functions and considering stochasticity when integrated assessment models are used as decision tools" by Kopp, Hsiang and Oppenheimer (*15*). The work presented in the current Research Article represents new analysis and results that were not contained in either earlier text and which ultimately operationalizes the goals we outlined in the 2013 conference paper.

A Materials and Methods Overview

Climate model integration Probabilistic projections of daily temperature and precipitation were produced with the Surrogate/Model Mixed Ensemble (SMME) method (*19, 41*), which employs probabilistic projections of GMST change produced using a simple climate model (SCM) to weight the gridded temperature/precipitation projections from a multi-model ensemble of downscaled GCM output, and employs linear pattern scaling (*54*) to produce 'model surrogates' that cover portions of the SCM-derived GMST probability distribution not present in the GCM ensemble (spatial patterns of temperature shown in Figure 1A, precipitation shown in Figure S1). SCM temperature projections were produced using the MAGICC6 (*55, 56*), forced with Representative Concentration Pathway emissions (*20*) and with equilibrium climate sensitivity calibrated to match the assessment of ref. (*57*). The multi-model downscaled GCM ensemble (*58*) was produced using the Bias-Correction/Statistical Disaggregation method of GCMs participating in the Coupled Model Intercomparison Project (CMIP) Phase 5 project (*21*). In contrast to traditional pattern scaling, pattern scaling as employed in SMME to capture tails not represented in the CMIP5 archive retains unforced climate variability, which can substantially influence year-to-year weather. To produce station-level projections, model and model surrogate projections are anomalized with respect to their own historical records and then are added to observed temperature and precipitation normals (1981-2010) at stations from the Global Historical Climatology Network (GHCN) (*59*). Monthly averages are temporally disaggregated into daily realizations using historical weather variability (*60*). Each county is assigned station-level projections that are nearest its geographic centroid.

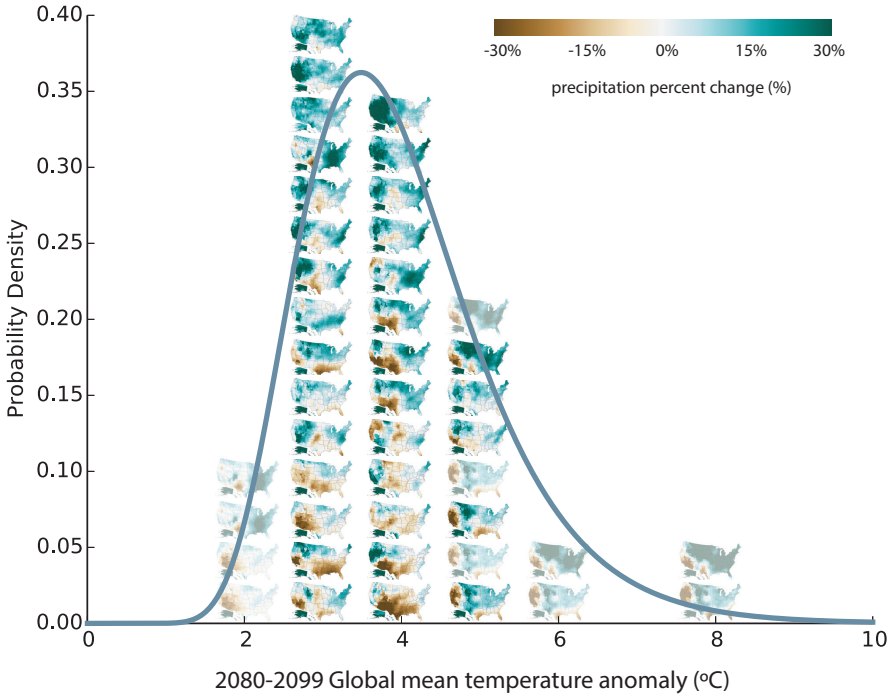

Supplementary Figure S1: **Distribution of Surrogate/Model Mixed Ensemble of precipitation projections as function of GMST anomaly.** 44 climate models (solid maps) and model surrogates (dimmed maps) are weighted so the distribution of the 2080–2099 GMST anomaly exhibited by weighted models matches the probability distribution of estimated GMST response (blue-grey line) under RCP8.5. Analogous display for temperature in Figure 1A.

Econometrically-derived impact integration Fifteen impacts are calculated using twenty-six dose-response functions from empirical econometric analyses that met specific methodological and sample criteria, in some cases with additional analyses from personal communication with authors (details in SOM B). Dose-responses functions are conditional probability distributions, $p(I|T_{\text{avg}}, T_{\text{max}}, T_{\text{min}}, P)$, for an impact I and daily mean (T_{avg}), maximum (T_{max}), and minimum (T_{min}) temperatures and precipitation (P). In cases where multiple estimates are available, we combine them for each set of conditioning variables values using hierarchical Bayesian modeling (*61*). We developed an collaborative online tool for this meta-analysis technique (`http://dmas.berkeley.edu`) to crowdsource future empirical analyses, facilitating updates to these results. See Sections B-C.

Projection calculation Impacts are calculated from the dose-response functions at the county-level for each year and reported as changes from 2012. In each RCP scenario, Monte Carlo (MC) sampling is used to account for uncertainty in climate realization uncertainty (RCP2.6: 29 climate realizations,

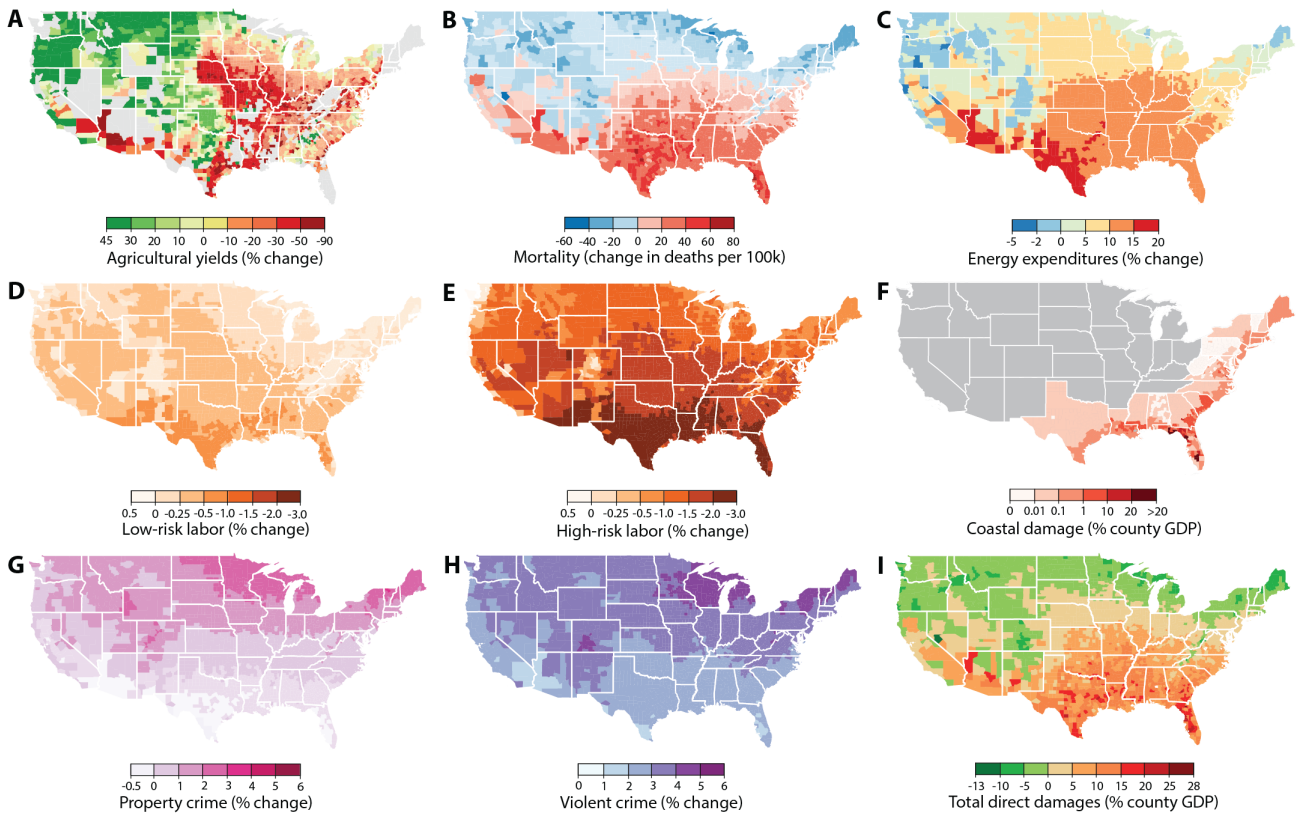

Supplementary Figure S2: **Spatial distributions of projected median damages by sector.** Same as Figure 2 in main text for median projections, but without significance levels indicated. County-level median values for average 2080-2099 RCP8.5 impacts using median dose-response functions. Impact changes are changes relative to counterfactual "no additional climate change" trajectories. Color indicates magnitude of impact in median projection. Negative damages indicate economic gains. **(A)** Percent change in yields, area-weighted average for maize, wheat, soybeans, and cotton. **(B)** Changes in all-cause mortality rates, across all age groups. **(C)** Change in electricity demand. **(D)** Change in labor supply of full-time equivalent workers for low risk jobs where workers are minimally exposed to outdoor temperature. **(E)** Same as (D) except for high risk jobs where workers are heavily exposed to outdoor temperatures. **(F)** Change in damages from coastal storms. **(G)** Changes in violent crime rates. **(H)** Changes in property crime rates. **(I)** Median total direct economic damage across all sectors (A)-(H).

RCP4.5: 43, RCP8.5: 44), within-month weather uncertainty (10 draws), and econometric uncertainty (25 quantiles). Thus, we calculate $116 \times 10 \times 25 = 29,000$ possible values for each of the 15 impacts in each of 3,143 counties in each year 2000–2099 (distributions of end-of-century impacts in counties shown in Figure 2 and median projections shown in Figure S2). State and national impacts are weighted averages over counties. Impact distributions are computed as empirical distribution functions. See SOM D-E.

Uncertainty decomposition Within RCP8.5, the climate realization, within-month weather draw, and dose-response function quantile are sources of uncertainty. We calculate the variance across impacts, varying each of these three individually and holding the others at a baseline. The *interaction component* in Figure S6 is the total variance minus the sum of the remaining variances. Mathematical derivations are in Section F.

Energy impacts The direct costs and benefits of climate-driven change in energy demand were assessed using RHG-NEMS, a version of the National Energy Modeling System (NEMS), developed by the U.S. Energy Information Administration (*62*), maintained by the Rhodium Group (RHG). RHG-NEMS is a detailed, multi-sector, bottom-up model of U.S. energy supply and demand linking residential, commercial, and industrial demand, electricity and primary energy supply, and macroeconomic feedbacks, among other factors. Because of the complexity and run time of RHG-NEMS, we used representative climate scenarios to construct region-specific response functions linking energy expenditures to changes in climate. These impact functions were applied to compute county-level heating degree-day and cooling degree-day data and were then aggregated using spatially-explicit energy expenditure data (*63, 64*). See Section G.

Coastal impacts Damages from MSL interacting with cyclones are computed using the Risk Management Solutions (RMS) North Atlantic Hurricane Model and U.S. Winter Storm Model. Stochastic spatial Markov models semi-parametrically fitted to historical storm tract data (*34*) are used to construct a large ensemble of storm tracks, including genesis and lysis. For tropical cyclones, analytical wind field profiles (*32*) are used to compute 10-meter, three-second peak gusts on a variable resolution grid for each storm. Wind and pressure fields, over the lifetime of the storm, are used to force the MIKE 21 hydrodynamic model system (*33*) to estimate storm surges and wave impacts. Damages from both wind fields and storm surges are estimated based on engineering-based models of vulnerability calibrated to historical statistical relationships between exposure and historical damage, where the location, elevation, and value of exposed assets are drawn from a proprietary RMS data base of all individual buildings along the Atlantic Coast. Impacts of MSL are simulated by imposing MSL projections derived from ref. (*36*) and differencing storm losses from simulations without MSL. Changes in hurricane frequency and inten-

sity are accounted for by adjusting the rate of storm genesis and intensification to match distributions of tropical cyclone projections from ref. (*35*) for RCP8.5 and (*65*) for RCP4.5, and then differencing losses from baseline simulations. See Section H.

Aggregate damage function construction Total damages in each sector and each daily projection are valued and aggregated nationally. Each of these aggregate outcomes are then indexed against ΔGMST in the corresponding climate realization. OLS or quantile regressions are used to characterize the joint distribution of aggregate impact realizations and ΔGMST across the three RCPs. The procedure is similarly implemented for total direct damages to compute the aggregate economy-wide damage function. It is then possible to adjust this damage function to account for social valuations of risk and inequality. See Sections I-K.

Dynamic computable general equilibrium modeling Temporal dynamics and general equilibrium effects of direct damages were modeled using a dynamic recursive computable general equilibrium (CGE) model, the RHG Model of the U.S. Economy (MUSE) (*41*). The model is calibrated using 2011 social accounting matrices (*66*) and solves for market-clearing prices and quantities simultaneously at the NCA-region level for multiple production sectors, households, and government agents. The model tracks investment by region and sector and tracks changes in productivity, age-specific population, and capital stock by vintage, region, and sector over time. Energy expenditure and labor productivity impacts are implemented as changes in input factor productivity for producers and consumers using these goods. Agricultural yield impacts are represented as changes in the output productivity of the relevant agricultural goods, after storage is accounted for using an empirical auto-regressive model. Coastal damages are represented as reductions in vintaged capital stock and mortality affects the time series of population projection for the age cohorts in which deaths (or reductions in deaths) occur. See Section L.

B Micro-founding climate impacts with econometric results

We develop empirical, micro-founded sector-specific damage functions for a number of sectors seen to be economically important. These comprise agriculture, crime, health, labor, and electricity demand. Within

each sector, we draw on statistical studies that robustly account for a number of potential confounding factors when trying to identify the impacts of climate. Numerous high-quality and insightful studies are omitted from our analysis because they did not meet all of our criteria, although many studies were used to confirm the validity reported findings of the selected studies. Notably, however, we have designed our approach to be *dynamically inclusive in the long-run* by building a system for crowd-sourced meta-analysis and collaboration. Incorporating each study took considerable effort, often requiring new data, efforts on the part of the original authors and ourselves to rerun analyses, and extensive discussions to ensure an accurate interpretation of results. In this process, we are indebted to the authors of the analyzed studies.

We applied the following criteria in assessing studies:

1. **Nationally representative**. We required that studies be conducted at national level or be drawn from a representative random sample of the entire US. This was of particular relevance to health studies. For example, many studies that we considered performed detailed time-series analysis of single or multiple cities (e.g., (*67*); (*68*)). While these were high-quality studies, inclusion would have required either a weighting scheme based on city populations or an assumption of national generalizability.

2. **Analyze recent time-periods in US history**. As we are concerned with potential effects of adaptation, we preferred studies that identified effects as close to the present as possible.

3. **Robust to unobserved factors that differ across spatial units** (jurisdictions, counties, or states). We placed an emphasis on studies that were able to control for unobservable differences between spatial units of analysis with the inclusion of fixed effects. This required the use of longitudinal or panel data, as cross-sectional comparisons between could suffer from omitted variable bias.

4. **Identify responses to high-frequency (daily or weekly) climate variables**. The importance of using high-frequency data to estimate climate impacts is demonstrated by all papers included, building on early work by (*50*), and in one case finding large effects by considering sub-daily temperature responses (*22*).

5. **Identify responses to the full distribution of temperature and rainfall measures**. Many studies looked at single climatic events, or parts of the temperature or rainfall distribution (e.g., heatwaves in (*69*)). As we are modeling annual impacts, we chose only those studies that included the full distribution of realised climate outcomes, and ensured the validity of results by comparison to numerous studies looking at single phenomena or sub-populations.

6. **Account for seasonal patterns and trends in the outcomes**. Cyclicity and seasonality of responses to climate forcings are sources of major concern, so we selected only those studies that robustly accounted for seasonal patterns and time trends in their analysis.

7. **Ecologically valid**. We required studies to be valid for real-life circumstances and levels of exposure, which led us to prefer studies that were quasi-experimental in design, using observational data. For example, in the case of labor, numerous laboratory studies exist on the intensive margin effects of temperature upon productivity (e.g., (*70*)). As these raised a question of ecological validity when applied to the labor sector, we chose to not include them.

Many of the impacts of climate change will unfold over years, but distinguishing between the role of climate change and the role of social, technological, and economic evolution is very difficult over any long time horizon. Our criteria for selecting studies requires that long-term trends are accounted for and are not reflected in the measured impact response functions. As a result, the impacts that we measure are from idiosyncratic distortions in the weather distribution that are orthogonal to long-term trends (*13*). This approach has both strengths and weaknesses. Its key strength is that it clearly identifies the impacts of weather as distinct from longer-term changes. Importantly, it only requires the weakest form of the *unit homogeneity assumption* among all approaches used to measure climate impacts empirically (*13*). However, it may miss many of the long-term impacts of climate change, such as impacts on groundwater supplies.

Numerous previous authors have incorrectly stated that this approach only identifies the effect of weather and not the effect of climate. The assumptions necessary for these studies to be valid are derived and analyzed in (*13*). Notably, the key assumption for these approaches to be valid is the *marginal treatment comparability assumption*, which requires that "the effect of a marginal change in the distribution

of weather (relative to expectation) is the same as the effect of an analogous marginal change in the climate" (*13*). We refer readers interested in this method and discussions or tests of necessary assumptions to (*13*).

We identify a number of studies using panel data to isolate the variation within the relevant spatial unit, while controlling for unobservable difference between units. Estimates from each of the studies were combined, as detailed in section C. We have been conservative in our choice of studies for the current analysis, using only studies which we think most credibly identify the impact of climate upon specific outcomes in each sector. However, our approach allows for future studies to be incorporated, introducing new findings, and modifying the current results. The following is a complete list of empirical response functions used in this study, with detailed discussion of each of the studies beneath:

Agriculture	Maize yields vs. temperature (East)
	Maize yields vs. temperature (West)
	Maize yields vs. precipitation (East)
	Maize yields vs. precipitation (West)
	Wheat yield vs. temperature
	Soybean yields vs. temperature (East)
	Soybean yields vs. temperature (West)
	Soybean yields vs. precipitation (East)
	Soybean yields vs. precipitation (West)
	Cotton yields vs. temperature
	Cotton yields vs. precipitation
	Maize yields vs. 100ppm CO_2 increase
	Wheat yields vs. 100ppm CO_2 increase
	Soybean yields vs. 100ppm CO_2 increase
	Cotton yields vs. 100ppm CO_2 increase
Crime	Violent crime vs. temperature
	Violent crime vs. precipitation

	Property crime vs. temperature
	Property crime vs. precipitation
Health	Mortality vs. temperature (all age)
	Mortality vs. temperature (younger than 1 year)
	Mortality vs. temperature (1 - 44 years)
	Mortality vs. temperature (45 - 64 years)
	Mortality vs. temperature (65 years and up)
Labor	Hours worked in high-risk industries vs. temperature
	Hours worked in low-risk industries vs. temperature

B.1 Agriculture

Schlenker and Roberts (*22*)

Outcome data:	Yields for maize, soybeans, and cotton from US Department of Agriculture National Agricultural Statistical Service.
Climate data:	PRISM temperature and rainfall, spatially and temporally interpolated from station data to daily resolution in each county.
Sample period:	1950-2009
Sample unit:	County-years, for counties with recorded yields of maize, soybeans, or cotton
Methodology:	Piecewise linear response of log(yield) to cumulative temperature (degree days) and polynomial response to precipitation (seasonal total), controlling for county fixed effects and state-specific quadratic trends. Piecewise linear models are specific to each crop type, with thresholds that capture the beneficial effects of temperatures below a certain point, and the deleterious effects above.
Result:	Modified version of (*22*) (SI Appendix, p. 9, fig. A3; and p. 20, fig. 10).

Impact function: We contacted the authors of the study to select a preferred response function from the multiple methods they had employed, selecting a piecewise-linear specification using degree days for temperature and seasonal total precipitation. We obtained impact functions for each of the three crops studied, for both temperature and precipitation. The authors note the distinct difference in response between counties to the east and west of the 100th meridian for maize and soybeans, so we obtained separate response functions in for these regions. On December 19th, 2013, we were sent a complete list of response functions that were updated span the time period up to and including 2011 (as presented in (*71*)).

Hsiang, Lobell, Roberts, and Schlenker (*72*)

Outcome data:	USDA-NASS
Climate data:	University of Delaware monthly temperature and precipitation
Sample period:	1950-2007
Sample unit:	County-year
Methodology:	Non-linear response of log(yield) to crop-specific seasonal average temperature and precipitation, controlling for county and year fixed effects.
Result:	(*72*) (p. 5).
Impact function:	We use the response of wheat to seasonal average temperature presented in the paper. Results were obtained from the authors. Calorie-weighted averages were taken between maize and wheat in order to combine results, as detailed in section D.

McGrath and Lobell (*23*)

Outcome data:	Yield from 1960-2004 from FAOStat.
Climate data:	Keeling CO_2 concentrations and country average P/PET.

Methodology:	Process model that develops the response of different crops to carbon dioxide concentrations and growing season P/PET from empirical studies. This is then used to estimate the changes to historical yields under a 100ppm increase in CO_2.
Result:	(*23*) (p. 5, fig. 4, obtained US result from authors).
Impact function:	We contacted the authors and received estimates of the CO_2 fertilization relationship with yields of different crops on January 17th, 2014, specifically for the US. Data were for 8 different crop types. We used an average of all types for cotton estimates.

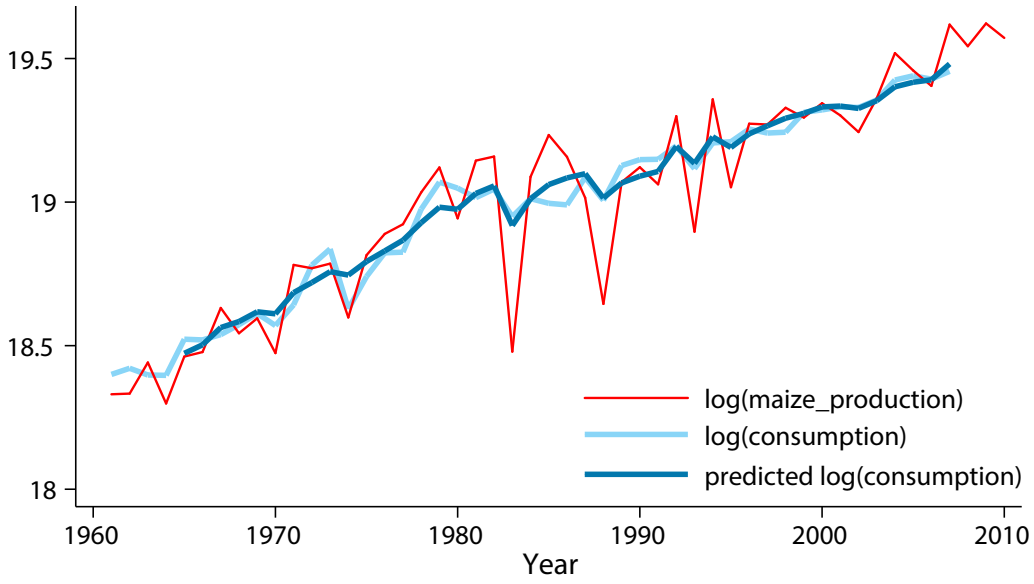

Supplementary Figure S3: Predicted consumption of maize, modeled as a moving average of production. Predicted values compare well to observed consumption, and allow us to project the smoothed consumption values out to the end of the century.

B.1.1 Storage

In addition to the above impacts on yields, we observe that farmers store crops for sale in the future, and so the overall impact of climate on supply of crops may appear smoother than if there were no storage. For our projections, we also make use of Fisher et al. ((*73*), Appendix p.xi, table A4) to estimate crop consumption as a moving average process of crop production. We estimated the following equation for

crop c,

$$\ln(consumption)_{c,t} = \sum_{l=0}^{L} [\beta_{c,l} \times \ln(production)_{c,t-l}] + \theta_c t + \gamma_c t^2 + \epsilon_{c,t}$$

where t indexes years and $L = 2$, except for soybeans where $L = 3$, and we account for linear (θ_c) and quadratic (γ_c) time-trends. Example results of this model are shown in Figure S3. We project the smoothing of future crops with a time-series structure that incorporates these empirical results on storage. Weights for each crop are constructed from the lagged coefficients, β_l, presented in Section D.1.

B.2 Crime

Jacob, Lefgren, and Moretti (*26*)

Outcome data:	FBI National Incident Based Reporting System
Climate data:	Weekly temperature and precipitation from the NCDC GHCN-Daily database.
Sample period:	1995-2001
Sample unit:	Jurisdiction-weeks
Methodology:	Linear response of log(crime_rate) to average temperature and precipitation, controlling for jurisdiction-by-year and month fixed effects, as well as jurisdiction-specific 4th order polynomials in day of year.
Result:	Modified version of (*26*) (p. 508-509, table 2).

Impact function: We obtained data and replication files from the authors and generated coefficients for a month-long exposure window, to account for displacement of crime, as noted in the text. The climate variables are at weekly resolution, and in order to make this comparable to (*27*) we reran the analysis using maximum temperatures and then scaled the coefficients in (*26*). We did this by first dividing the coefficient for the monthly exposure by 7, to get a daily response, and further by 4 to account for the lagged climate variables. This resulted in the marginal effect on crime of a 1°F increase in daily temperature. Taking a reference point of zero response at a temperature of 65°F (to coincide with the central point of the reference bin of (*27*)) we derived a linear response of violent crimes and property crimes to temperature and precipitation.

Ranson (*27*)

Outcome data: FBI Universal Crime Reporting Data.

Climate data: Daily temperature and precipitation from the NCDC GHCN-Daily database.

Sample period: 1960-2009

Sample unit: County-months

Methodology: Non-linear response of log(crime_rate) to maximum temperature and precipitation, controlling for county-by-year and state-by-month fixed effects. Temperature is transformed into number of days within 10°F bins, with the 60-69°F bin as a reference point.

Result: (*27*) (p. 9, fig. 4).

Impact function: We contacted the author and received updated estimates of the percentage change for each of 8 different classes of crimes on March 12th, 2014. To derive response functions, we grouped these into violent crimes (murder, rape, aggravated assault, and simple assault) and property crimes (robbery, burglary, larceny, and vehicle theft), and combined results within each class of crimes.

B.3 Health

Deschenes and Greenstone (*24*)

Outcome data:	National Center for Health Statistics Compressed Mortality Files.
Climate data:	Daily temperature and precipitation from NCDC
Sample period:	1968-2002
Sample unit:	County-years
Methodology:	Non-linear response of mortality to temperature, controlling for county-by-age-group and state-by-year-by-age-group fixed effects. Temperature is transformed into number of days in an year-long window within 10°F bins, with the 50-59°F bin as a reference point.
Result:	Modifed version of (*24*) (p. 9, fig. 2).
Impact function:	We contacted the authors and received estimates on November 5th, 2013. To make the study comparable to Barreca et al. (*25*), the main analysis was rerun with log(mortality) as an outcome.

Barreca, Clay, Deschenes, Greenstone, and Shapiro (*25*)

Outcome data:	Mortality from the Mortality Statistics of the US (pre-1959) and the Multiple Cause of Death files (post-1959).
Climate data:	Daily temperature and precipitation from the NCDC GHCN-Daily database.
Sample period:	1929-2004
Sample unit:	State-months
Methodology:	Non-linear response of log(mortality) to temperature, controlling for state-by-month and year-month fixed effects, and state-by-month-specific quadratic time trends. Temperature is transformed into number of days in a two-month window within 10°F bins, with the 60-69°F bin as a reference point.
Result:	Modified version of (*25*) (p. 37, table 3, panel B).

Impact function: We contacted the authors and received estimates on 5th November, 2013. The preferred specification, to account for forward displacement, was to use monthly mortality with a 2-month exposure window to temperature. We used the estimated response from 1960-2004. To make this response comparable to the response of Deschenes and Greenstone (*24*), the analysis was rerun with the reference point changed to the 50-59°F bin. To scale the coefficients, we divided each coefficient value by a factor of six. We also obtained age-specific response functions for ages 0-1, 1-44, 45-64, and 65+.

B.4 Labor

Graff Zivin and Neidell (*28*)

Outcome data:	Hours worked from the American Time Use Survey.
Climate data:	Daily temperature, precipitation, and humidity from NCDC.
Sample period:	2003-2006
Sample unit:	Person-days
Methodology:	Seemingly-unrelated regression allowing for correlated errors between time spent working, or indoor and outdoor leisure. Non-linear response to maximum temperatures controlling for county, year-by-month, and day of week fixed effects, as well as individual level controls. Temperature is transformed into number of days within 5°F bins, with the 76-80°F bin as a reference point. High-risk sectors of the economy are defined as Agriculture, Forestry, Fishing and Hunting; Mining, Quarrying, and Oil and Gas Extraction; Utilities; Construction; and Manufacturing.
Result:	High-risk: (*28*) (p. 15, fig. 3); Low-risk: (*28*) (p. 16, fig. 4)
Impact function:	We contacted the authors prior to publication and received full estimates for high-risk and low-risk labor responses to temperature on December 18th, 2013.

C Meta-analysis approach

The dose-response functions are treated as probability distributions conditioned on weather variables, such as temperature and precipitation. In the generic case, denoting weather variables as H and the impact on an outcome of interest I, then the dose response function is

$$I = \gamma(H)$$

where it is understood that $\gamma(.)$ is only known with uncertainty. This representation allows us to account for the range of uncertainty in previously published empirical estimates and motivates meta-analysis to synthesize previous studies that are uncertain and may not agree perfectly with one another. In this analysis, we note that some dose-response functions are based on a single study; others combine results from more than one study.

The impact estimates that combine results from multiple studies apply a Bayesian hierarchical model structure (*61*). This approach simultaneously estimates a distribution of possible underlying effect sizes, as well as a degree of partial pooling. To the extent that the individual study estimates are consistent with a single underlying effect, their estimates are pooled to accurately estimate the effect. However, to the extent that the study estimates are inconsistent with each other, the hierarchical model determines a study-specific idiosyncratic effect. The interpretation of this model averaging procedure is discussed in detail in the context of climate impact estimation in (*30*).

Consider a collection of impact functions, $z_i(\beta_i|H)$, with H representing weather variables and $i \in \{1, \ldots, N\}$ indexing independently published results. The variable β_i is an estimate of a true (unobserved) parameter θ_i that characterizes the response for study i. The true parameter combines both a common effect, reflected by the hyperparameter μ, and a study-specific effect $\theta_i - \mu$. We wish to combine the estimates β_i into a single generalizable conditional distribution that only captures the effect that is common across studies, $\gamma(\mu|H)$. We treat each value of H independently, so we will write these functions as $z_i(\beta_i)$ and $\gamma(\mu)$.

The conditional parameter distributions are assumed Gaussian

$$\theta_i|\mu,\tau \sim \mathcal{N}(\mu,\tau^2)$$
$$\beta_i|\theta_i \sim \mathcal{N}(\theta_i,\sigma_i^2).$$

Accordingly, $\beta_i|\mu,\tau \sim \mathcal{N}(\mu,\tau^2+\sigma_i^2)$. We are interested in estimating the underlying hyperparameter μ and the between-study variance τ^2, which involves assessing their joint posterior probability distribution

$$p(\mu,\tau|\beta,\sigma) = p(\mu,\tau)\prod_{i=1}^{N}\frac{p(\beta_i|\mu,\tau,\sigma_i)}{p(\beta_i|\sigma_i)}.$$

We apply non-informative uniform priors $\mu \sim Unif(-\infty,\infty)$ and $\tau \sim Unif(0,\infty)$. The values of β_i and σ_i^2 are provided by the published studies, and the rest of the parameters are simultaneously estimated.

An analytic solution exists for how to generate draws from the posterior distribution of this hierarchical model, and is described in chapter 5 of Gelman *et al.* (*61*). We approximate the posterior by producing draws and constructing a histogram for each conditional distribution, as follows. First, we compute $q(\tau|\beta,\sigma) \propto p(\tau|\beta,\sigma)$ on a 100-point grid between 0 and twice the greatest standard error, using

$$q(\tau|\beta,\sigma) = V_\mu^{1/2}\prod_{i=1}^{N}(\sigma_i^2+\tau^2)^{-1/2}\exp\left(-\frac{(\beta_i-\hat{\mu})^2}{2(\sigma_i^2+\tau^2)}\right)$$

where $\hat{\mu} = \frac{\sum_{i=1}^{N}\frac{1}{\sigma_i^2+\tau^2}\beta_i}{\sum_{i=1}^{N}\frac{1}{\sigma_i^2+\tau^2}}$ and $V_u^{-1} = \sum_{i=1}^{N}\frac{1}{\sigma_i^2+\tau^2}$. We then construct the empirical CDF of $\tau|\beta,\sigma$ from these samples, and use the inverse CDF method to create draws from this distribution. For each draw of τ, we compute the draws from the conditional posterior distributions $\mu|\tau,\beta,\sigma \sim \mathcal{N}(\hat{\mu},V_\mu)$.

All empirically derived dose-response functions after meta-analysis (where multiple studies were available) are shown in Figure S4.

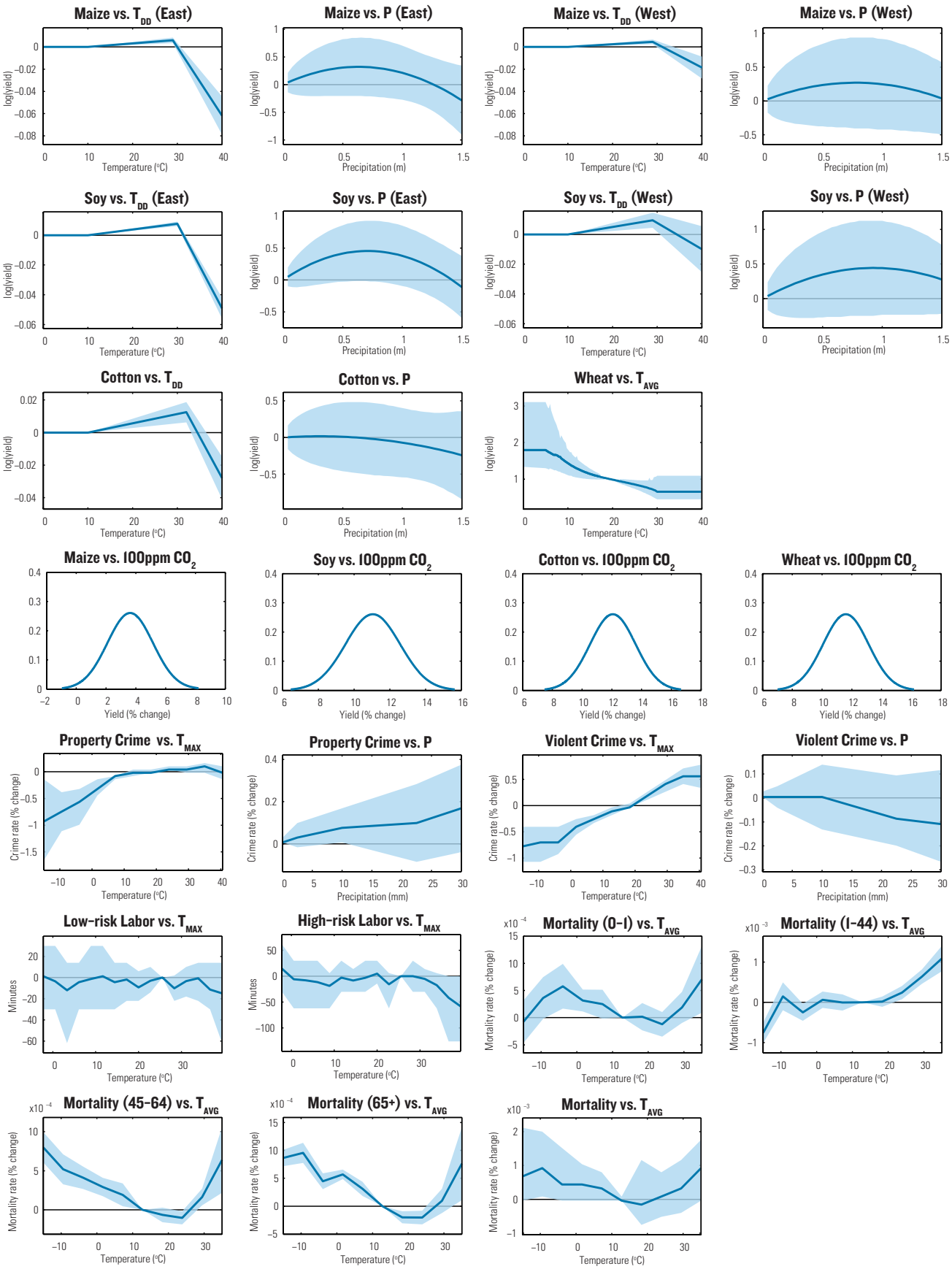

Supplementary Figure S4: **All 26 dose-response functions used in our analysis, following Baysian model averaging in cases where multiple findings are reported.** Solid lines are medians of the conditional posterior, 95% credible intervals are shaded.

D Applying climate projections to econometric dose-response functions

For each county and each year, we apply the full range of *climate realizations* and *weather projections* for each RCP scenario to the 26 composite (posterior) dose-response functions for each sector (shown in Figure S4) for each day of each projection, accounting for the statistical uncertainty in the dose-response functions. For a given outcome, the impact I for county j in year t depends on

- the RCP scenario r
- the climate realization m
- the daily projection w, and
- the empirical quantile of the dose-response function k.

Weather realizations are resolved for each day d, where $d \in t$ denotes days that occur in year t. We apply the weather variables $H^{rmw}_{j,d\in t}$ to each composite dose-response function $\gamma(.)$ to recover annual impacts for a given county:

$$I^{rmwk}_{jt} = \gamma\left(\mu^k | H^{rmw}_{j,d\in t}\right)$$

where the superscripts denote the state of the world (RCP scenario-by-climate realization-by-weather projection-by-quantile) in a specific projection and subscripts denote the time (year) and place (county) for which the outcome is recorded.

In total, we build projections for three RCP scenarios (2.6, 4.5 and 8.5) which each have a large number of climate realizations that are the climate models and climate model surrogates used to reconstruct the distribution of GMST change (29 climate realizations for RCP 2.6, 43 for RCP 4.5 and 44 for RCP 8.5) for a total of 116 climate realizations. The differing number of climate realizations reflects the different numbers of modeling teams that generated climate forecasts for the CMIP5 scenarios. Note that within each RCP, each climate realization is assigned a weight Ω^{rm} so that the full weighted distribution of realizations mirrors the distribution of climate sensitivities (*19, 41*) (recall Figure 1A). Each climate realization is utilized to construct ten daily projections by resampling daily weather residuals (relative to

monthly climatologies) from the historical record in yearly blocks (to ensure autocorrelation structures are preserved). We then implement Monte Carlo resampling (described further below) of the empirical response functions to construct twenty five versions of each of the 26 dose-response functions, indexed by k, for each daily projection. Thus, we calculate $116 \times 10 \times 25 = 29,000$ possible values for each of the 15 impacts in each of the 3,143 counties in each year (2013-2099). These possible future impacts for each county-year represent a range of outcomes for each location and each moment in time, which we use to construct conditional probability distributions for outcomes at those locations and times (described in Section E).

Monte Carlo Our Monte Carlo approach captures the full range of uncertainty in dose-response function estimates, under the assumption that each function is independent (in the sense of its statistical uncertainty). We randomly select quantiles, indexed by k, for each of the 26 empirical distributions shown in Figure S4. (When specified, such as when we analyze uncertainty, only the median quantile is used for all or some of these dose response functions.) The ordinality of the quantiles is chosen so that these describe, in essence, low, median, and high impact scenarios. High quantiles correspond to greater losses in yield and labor productivity, and greater increases in crime and mortality, within the range of statistical uncertainty. The same quantile is used across the entire range of the conditioning variable. By evaluating each impact function at a quantile, we generate a single-dimensional, deterministic function which is used in the evaluation of the impact for each Monte Carlo run.

Below, we explain how I is computed for each impact, drawing on the structure of results recovered from the literature (Section B) and our meta-analysis (Section C). We use the notation T_{AVG} for mean daily temperature; T_{MIN} and T_{MAX} for minimum and maximum daily temperature, respectively; and P for for precipitation. $f(.)$ and $g(.)$ are generic notations for functions that are described in each subsection.

Note that the impact results for crime, labor productivity, and mortality are all estimated by binning weather values into discreet bins (*13*), since this is the model utilized in the previous analyses that we draw on. In these cases, we construct a continuous impact curve by linearly interpolating between the midpoints of these bins.

Throughout, impacts are ultimately reported relative to 2012, the baseline year. The definitions of each impact below do not reflect this.

D.1 Agricultural Yields and Production

Percent changes in agriculture production, relative to 2012, were generated using fixed, county-specific growing seasons. The growing season, denoted $S(j)$ for county j, is determined using the centroid of the county applied to the planting and harvesting dates in (*74*). Denote $S(j) \cap t$ as the set of days in year t that are in the growing season. For maize and wheat, for which (*74*) provides two calendars (two croppings for maize, and summer and winter wheat), the calendar that represented the greatest portion of land area in each county was used.

Relative changes in yield are calculated based on seasonal temperatures and precipitation as follows:

Wheat Wheat uses a seasonal average temperature response function:

$$Y_{jt} = f\left(\frac{1}{N(S(j))}\sum_{d \in S(j)\cap t} T_{AVG,d}\right)$$

where $f(\cdot)$ is calculated by (*72*), as a function of average mean daily temperature over the growing season, and $N(S(j))$ is the number of days in the growing season for county j. This functional form was only used for wheat, since a degree-day representation was unavailable.

Cotton Cotton uses a single degree-day function:

$$Y_{jt} = e^{f\left(0.01\sum_{d\in S(j)\cap t} DD_{low}(T_{MAX,d},T_{MIN,d}),0.01\sum_{d\in S(j)\cap t} DD_{high}(T_{MAX,d},T_{MIN,d})\right)+g\left(1\times 10^{-3}\sum_{d\in S(j)\cap t} P_d\right)}$$

where DD_{low} and DD_{high} are growing degree days below and above the crop-specific breakpoint specified in (*22*), and calculated as specified there using the minimum and maximum daily temperatures. The functions $f(\cdot)$ and $g(\cdot)$ translate degree days and precipitation, respectively, into yield effects.

Maize and Soybeans Maize and soybeans have two degree-day responses:

$$Y_{jt} = \begin{cases} e^{f_{east}\left(0.01\sum_{d\in S(j)\cap t} DD_{low}(T_{MAX,d},T_{MIN,d}),0.01\sum_{d\in S(j)\cap t} DD_{high}(T_{MAX,d},T_{MIN,d})\right)+g_{east}(1\times 10^{-3}\sum_{d\in S(j)\cap t} P_d)} \\ e^{f_{west}\left(0.01\sum_{d\in S(j)\cap t} DD_{low}(T_{MAX,d},T_{MIN,d}),0.01\sum_{d\in S(j)\cap t} DD_{high}(T_{MAX,d},T_{MIN,d})\right)+g_{west}(1\times 10^{-3}\sum_{d\in S(j)\cap t} P_d)} \end{cases}$$

Here, $f_{east}(\cdot)$ and $g_{east}(\cdot)$ are used to the east of the 100th meridian, excluding Florida. In this areas, irrigation is less common and the response to increased temperatures is more extreme.

CO_2 fertilization is modeled as a multiplicative factor applied to yields, and estimated as a linear increase for each additional 100 ppm of CO_2:

$$Y'_{jt} = Y_{jt}\left(1 + \frac{[CO_2]_t - [CO_2]_{2012}}{100}\zeta\right)$$

where $[CO_2]_t$ is the CO_2 concentration in year t under a given RCP, and ζ is the estimated CO_2 fertilization effect, which varies from 3% to 12% depending on the crop, from (*23*). (*23*) does not provide a value for cotton, so the Bayesian combination of all provided crop effects is used for it.

As explained in Section B.1.1, economic output from the agricultural sector is not synonymous with yield due to storage. For each crop, we model output as a distributed lag function of yields

$$I_{jt} = \sum_{L=0}^{3} \lambda_L Y_{j,t-L}$$

where the coefficients λ_L are estimated from USDA data following (*73*) and described in Section B.1.1. This leads to output that is less variable than yields (recall Figure S3).

D.2 Crime

Both violent and property crime are calculated as,

$$I_{jt} = \left(1 + 0.01\frac{1}{12}\sum_{d\in t} f(T_{MAX,d})\right)\left(1 + 0.01\frac{1}{12}\sum_{d\in t} g(P_d)\right)$$

where $d \in t$ is the set of days in year t, $f(\cdot)$ is a function of daily maximum temperature, and $g(\cdot)$ is a function of daily precipitation. Both $f(\cdot)$ and $g(\cdot)$ are calculated as a Bayesian combination of the effect for each sub-category of crime estimated by (*27*) and the average effect for violent or property crime from (*26*).

D.3 Mortality

Both average and age-specific mortalities are calculated as,

$$I_{jt} = \sum_{d \in t} f(T_{AVG,d})$$

The parameters of $f(\cdot)$ are calculated as a Bayesian combination of the results from (*24*) and a corrected form of (*25*). Age-specific mortalities, for newborns, ages 1-44, ages 45-64, and ages 65 and up, are provided by (*25*).

Mortality is reported both as percentage changes, and as differences in the mortality rate. In either case, the pooled and age-specific mortality rates per county are from (*75*).

D.4 Labor Productivity

High-risk sectors of the economy are defined as Agriculture, Forestry, Fishing and Hunting; Mining, Quarrying, and Oil and Gas Extraction; Utilities; Construction; and Manufacturing. All others are considered low-risk. The structure of the labor productivity calculation is identical for high-risk and low-risk sectors:

$$I_{jt} = \frac{H + \frac{1}{60} \sum_{d \in t} f(T_{MAX,d})}{h}$$

where h is the average number of hours worked per year in the baseline. For high-risk labor, $h = 7.67 \times 365$, and for low-risk labor, $h = 6.92 \times 365$. The parameters of $f(\cdot)$ are provided by (*28*).

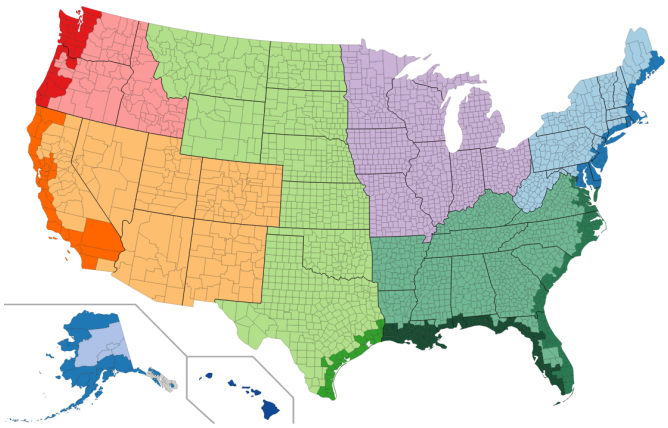

Supplementary Figure S5: Results were aggregated from county level to the modified NCA region level (one color per region) for passing to the CGE model (Alaska and Hawaii were not included in the CGE model results or national estimates, though impact results were calculated for them). Counties where coastal damages from storm surge and sea level rise are calculated are darkened.

E Probabilistic and aggregated econometrically-derived impacts

Within each RCP, climate realizations are weighted to capture the distribution of GMST changes, as described in (*19*). This allows the weighted distribution of projected outcomes to be interpreted as a probability distribution. This adjustment is important because climate model ensemble members are each individually "best guesses" and cannot be interpreted as unconditional independent draws from a true underlying probability distribution.

The probability distribution of impact I for a county j in year t for RCP scenario r is constructed by computing an empirical CDF for all the possible future realizations. When Ω^{rm} is the weight assigned climate realization m in RCP r by (*19*) (constraining $\sum_m \Omega^{rm} = 1$) then the CDF is

$$F_{it}^{r}(I) = \sum_{m}^{\bar{m}^r} \Omega^{rm} \sum_{w=1}^{10} \sum_{k=1}^{25} \frac{\mathbf{1}[I_{it}^{rmwk} \leq I]}{250}$$

where $\bar{m}$, the maximum index for m, is 29 for RCP 2.5, 43 for RCP 4.5, and 44 for RCP 8.5. Here, $\mathbf{1}[.]$ is the indicator function that is equal to one if the statement inside the brackets is true and zero otherwise. We are thus able to compute a full probability distribution of impacts for each county in each year, conditional on the emissions scenario. An identical calculation can be implemented for larger spatial units after aggregation, the only alteration to the calculation is that the index j is replaced by an

index for the more aggregated spatial unit (e.g., state).

Probability distributions for nationally aggregated impacts are reported in Table S1.

For many calculations, including the construction of national damage functions, impacts must be aggregated to a larger administrative unit than the county level. In the main text, results at the national level are used for Figures 5A-B, results at county-level are used for Figure 5C, and results at modified National Climate Assessment (NCA) region are used to calibrate damages in the CGE model used for Figure 5D. NCA region definitions used for the CGE model are shown in Figure S5 (note that due to the implementation of separate coastal damages in the CGE model, coastal NCA regions are split into a coastal portion and an inland portion).

To aggregate county-level impacts for impact I in state of the world $\{rmwk\}$ where J is the set of counties in the larger administrative units (J is the set of all counties in the national aggregate case), then the aggregated impact for year t is the weighted sum

$$I_{Jt}^{rmwk} = \frac{\sum_{j \in J} \omega_j I_{jt}^{rmwk}}{\sum_{j \in J} \omega_j}$$

where the weights must be chosen so that I_{Jt}^{rmwk} is a nationally meaningful number. Below we describe how the weights ω_j are selected for each sector.

E.1 Crop impacts aggregation

Following (*76*), grains yields (maize and wheat) are combined within the same county and aggregated to higher scales based on calorie totals. Within each county, the average impact is,

$$I_{jt}^{grains} = \frac{I_{jt}^{wheat} A_j^{wheat} C^{wheat} + I_{jt}^{maize} A_j^{maize} C^{maize}}{A_j^{wheat} C^{wheat} + A_j^{maize} C^{maize}}$$

where A_j^{wheat} is the average acres of wheat planted between 2000 - 2005, and A_j^{maize} is the average acres for maize. C^{wheat} and C^{maize}, the calorie density of wheat and maize, are 1690 calories/kg and 1615 calories/kg, respectively. The weighting of each county result for aggregation to larger administra-

tive units is

$$\omega_j^{grains} = A_j^{wheat} C^{wheat} + A_j^{maize} C^{maize}.$$

For cotton and soybean results, weights are simply the total area planted, as averaged over 2000 - 2005

$$\omega_j^{soy} = A_j^{soy}$$

$$\omega_j^{cotton} = A_j^{cotton}.$$

Because the impacts I in agriculture are yield changes, this approach recovers national average yields (calorie yields in the case of grains). To see this, denote yields y and note that national average yields in the baseline are

$$national\_yields^{pre} = \frac{\sum_j A_j y_j}{\sum_j A_j}$$

since total national production is $\sum_j A_j y_j$. After a change due to climate, national yields will be

$$\begin{aligned} national\_yields^{post} =& \frac{\sum_j A_j (y_j + \Delta y_j)}{\sum_j A_j} \\ &= \frac{\sum_j A_j y_j}{\sum_j A_j} + \frac{\sum_j A_j \Delta y_j}{\sum_j A_j} \\ &= national\_yields^{pre} + \frac{\sum_j A_j \Delta y_j}{\sum_j A_j} \end{aligned}$$

Thus, since $I_j = \Delta y_j$, then setting $\omega_j = A_j$ recovers the change in national yields.

E.2 Crime impacts aggregation

Percentage changes in crime are aggregated by setting ω_j to the number of reported property and violent crimes from the Uniform Crime Statistics, averaged over 2000 - 2005, and provided for reproduction of (*27*). Counties that are not explicitly identified at the county level (of which there are 172) are assigned the national average rates of property and violent crime.

E.3 Labor impacts aggregation

Labor supply impacts are aggregated by setting ω_j to the labor employment in each county averaged over 2000 - 2005, as reported by the Bureau of Labor Statistics (*77*). Following (*28*), this is done separately for high-risk industries, consisting of agriculture, forestry, fishing and hunting; mining, quarrying, and oil and gas extraction; utilities; construction; manufacturing; and transportation and warehousing. All other industries are considered low-risk. The BLS statistics exclude the counties represented by FIPS codes 02105, 02195, 02198, 02230, and 02275, since these were created after 2005.

E.4 Mortality impacts aggregation

Mortalities impacts are aggregated by setting ω_j to the 2010 census populations. All estimates (except for the NCA region estimates used to drive the CGE model) use total populations and the pooled mortality dose-response function.

For the aggregation from sub-NCA regions (in Figure S5) to NCA regions used in the analysis, the census totals for each age are summed into impact cohorts and used for weighting. This procedure is combined with using the age-specific dose-response functions. Tracking age is important in the CGE model because the number of years of future foregone earnings are used to value the cost of labor lost to mortality.

Supplementary Table S1: Weighted impact result percentiles

	RCP 8.5					RCP 4.5					RCP 2.6				
Percentiles	5	17	50	83	95	5	17	50	83	95	5	17	50	83	95
Agricultural Yields (%)															
2080-2099	-55.6	-41.7	-15.3	11.9	18.8	-43.1	-24.5	-3.4	6.1	10.4	-16.6	-11.5	-1.2	3.5	5.0
2040-2059	-19.7	-14.3	-3.3	7.4	11.8	-18.9	-12.7	-0.9	5.5	8.5	-13.1	-8.5	-1.8	3.2	5.3
2020-2039	-9.2	-6.5	-1.8	7.1	11.0	-11.3	-8.4	-0.6	6.2	9.2	-12.8	-6.9	-2.0	1.1	3.2
Agricultural Yields (%) (w/o CO_2fertilization)															
2080-2099	-69.1	-59.2	-40.0	-19.5	-15.5	-49.8	-33.3	-14.4	-6.0	-2.0	-19.1	-14.2	-4.3	0.4	1.7
2040-2059	-28.8	-24.0	-14.3	-4.8	-0.9	-25.1	-19.4	-8.4	-2.5	0.3	-16.8	-12.5	-6.0	-1.2	0.7
2020-2039	-13.3	-10.7	-6.3	2.3	6.0	-14.3	-11.5	-4.1	2.5	5.4	-15.5	-9.8	-5.0	-1.9	0.1
High Risk Labor (%)															
2080-2099	-3.2	-2.4	-1.4	-0.8	-0.6	-1.6	-1.1	-0.6	-0.2	-0.1	-0.6	-0.4	-0.3	-0.1	0.1
2040-2059	-1.1	-0.9	-0.5	-0.2	-0.1	-0.9	-0.7	-0.4	-0.1	0.0	-0.5	-0.4	-0.3	-0.1	0.1
2020-2039	-0.5	-0.4	-0.1	0.0	0.1	-0.5	-0.4	-0.2	0.0	0.2	-0.4	-0.3	-0.2	-0.1	0.1
Low Risk Labor (%)															
2080-2099	-0.8	-0.5	-0.2	-0.1	0.0	-0.3	-0.2	-0.1	0.0	0.0	-0.1	-0.1	0.0	0.0	0.1
2040-2059	-0.2	-0.2	-0.1	0.0	0.0	-0.2	-0.1	-0.1	0.0	0.0	-0.1	-0.1	0.0	0.0	0.0
2020-2039	-0.1	-0.1	0.0	0.0	0.0	-0.1	-0.1	0.0	0.0	0.1	-0.1	-0.1	0.0	0.0	0.1
Mortality (per 100,000 yr^{-1})															
2080-2099	0.6	3.7	9.5	20.8	35.6	-4.5	-2.5	1.0	5.9	11.9	-3.9	-2.3	0.8	3.2	5.0
2040-2059	-2.8	-0.5	2.9	6.6	10.1	-5.0	-3.2	-0.1	3.9	7.4	-3.3	-1.8	0.9	3.4	5.5
2020-2039	-3.4	-1.7	1.5	4.2	6.1	-5.1	-3.3	-0.6	2.3	5.5	-3.2	-1.8	1.2	3.0	5.7
Property Crime (%)															
2080-2099	0.3	0.4	0.7	1.0	1.1	0.0	0.1	0.5	0.9	1.0	-0.2	-0.1	0.2	0.5	0.7
2040-2059	-0.1	0.1	0.3	0.6	0.8	-0.1	0.0	0.4	0.7	0.8	-0.1	-0.1	0.2	0.5	0.6
2020-2039	-0.3	-0.1	0.0	0.4	0.5	-0.2	-0.1	0.2	0.5	0.6	-0.2	-0.1	0.1	0.3	0.4
Violent Crime (%)															
2080-2099	1.7	1.9	3.0	4.5	5.4	0.2	0.6	1.5	2.5	3.2	-0.2	-0.1	0.6	1.3	1.5
2040-2059	0.3	0.6	1.2	2.1	2.5	0.0	0.2	1.1	1.8	2.0	-0.2	0.2	0.7	1.1	1.5
2020-2039	-0.5	0.0	0.4	1.1	1.4	-0.4	0.0	0.6	1.1	1.3	-0.2	0.0	0.4	0.8	1.0

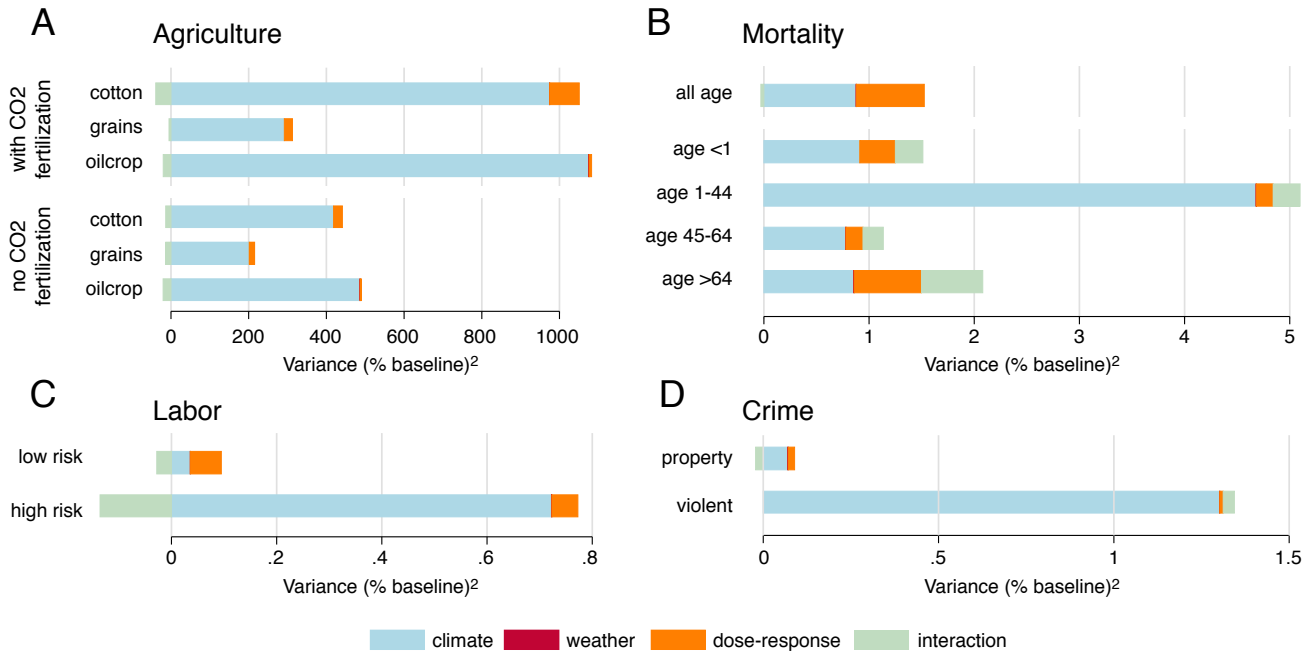

Supplementary Figure S6: **Decomposing sources of uncertainty for direct impacts.** Variance in 2080–2099 avg. direct impacts attributable to different sources of uncertainty under RCP8.5, identified by sampling single inputs one at a time while holding other inputs at median values. Units are in percent change over baseline in 2011 squared, since variances have squared units. "Climate" uncertainty comes from uncertainty in GMST and in the expected spatiotemporal distribution of weather conditional upon GMST, across climate realizations. "Weather" uncertainty comes from random within-month variations in weather that differ across daily projections within a climate realization. "Dose-response" uncertainty comes from statistical uncertainty in econometric estimates of dose-response functions. "Interaction" uncertainty is the residual variance (may be negative) relative to the variance when all factors are sampled simultaneously, which may be nonzero when nonlinear response functions interact with variance in model projections. Uncertainty in **(A)** agricultural impacts, with and without CO_2 fertilization, **(B)** heat-related mortality by age, **(C)** property and violent crime, **(D)** labor supply in high-risk and low-risk occupations.

F Decomposition of uncertainty for econometrically-derived impacts

Following the general framework laid out by ref. (*43*), we evaluate which sources of uncertainty contribute to the overall uncertainty of our projections for econometrically derived impacts in Figure S6. We focus our attention on understanding the variance

$$Var(I^{r=RCP8.5,mwk}_{J=national,t=2080-2099})$$

where the impacts are aggregated to the national level (J) for the period 2080-2099, as described in Section E. We restrict our attention to scenario (r) RCP 8.5.

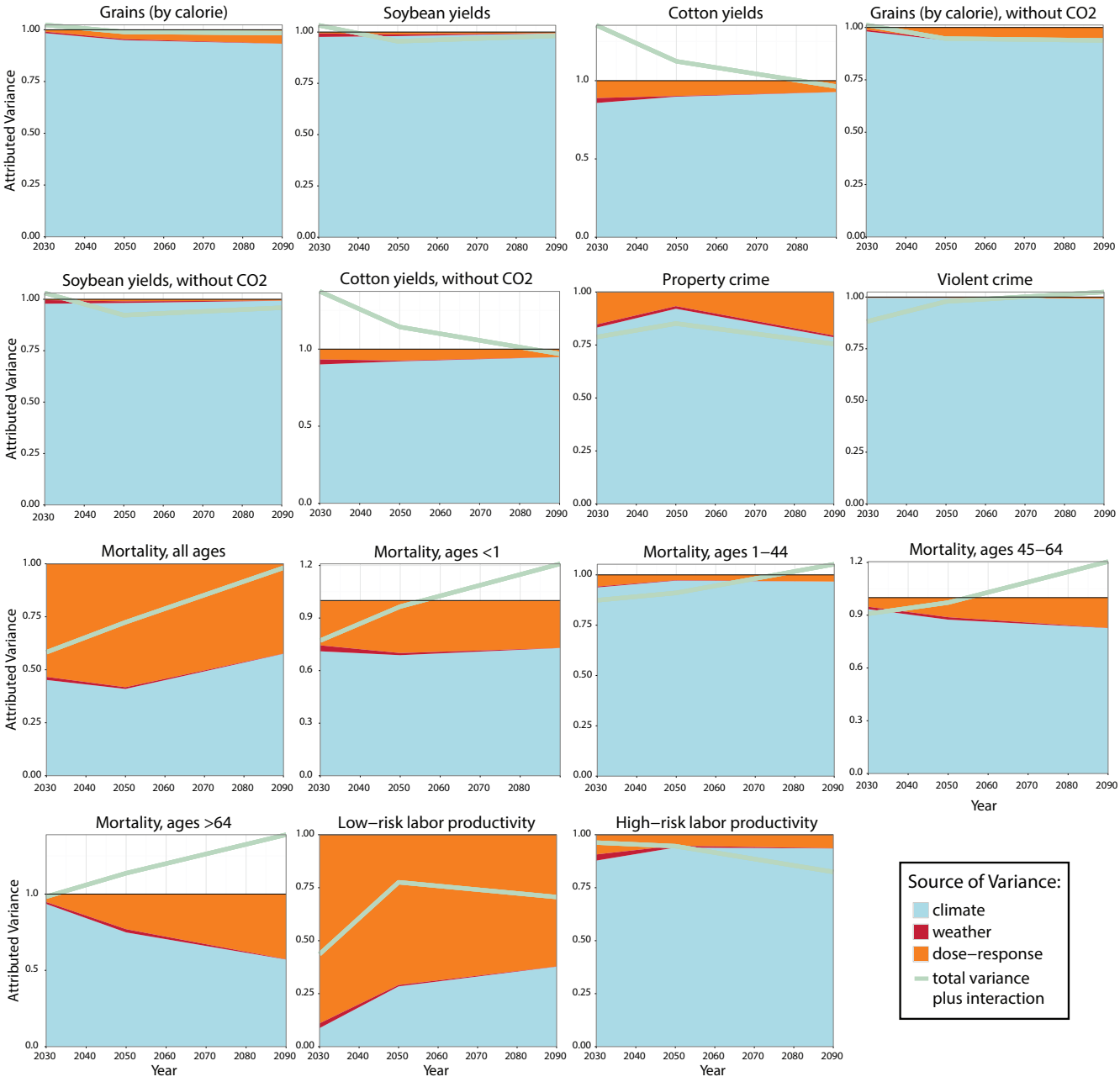

Supplementary Figure S7: **Decomposing sources of uncertainty for damages over time.** Same as Figure S6 but for multiple time periods and normalizing variances to by the sum of variances from climate models, weather, and econometric uncertainty. Approach is same as ref. (*43*). Green line indicates the total variance once the "interaction" component Λ is accounted for. Λ can be read as the difference between 1 and the green line at each moment, it is possible for $\Lambda < 0$.

We decompose the variance of impacts for the uncertain state of the world $\{mwk\}$ into contributions from the climate realization r, the daily projection w (largely due to within-month weather), and quantile k in the econometric model. To look at each of these contributions separately, we hold two of these sources of uncertainty fixed while allowing the third to vary. We do this procedure for each of three factors, and then compare the sum of these three marginal variances to the total variance. Any difference between the total variance and the sum of these three variances is attributed to interactions between sources of uncertainty, which may occur in cases where response functions are nonlinear (derived below). For the remainder of this section, we omit r, j and t super/subscripts for clarity, since they are held fixed throughout this portion of the analysis.

We are thus interested in decomposing the variance

$$Var(I^{mwk}) = Var(I^{mwk}|m, w) + Var(I^{mwk}|m, k) + Var(I^{mwk}|w, k) + \Lambda$$

where Λ is the term that emerges from the interaction of different sources of uncertainty. Specifically, we compute weighted empirical distributions over impacts for each of the following:

- Climate uncertainty, $Var(I^{mwk}|w = w_0, k = 50)$, from results for each climate realization m, of which there are 44 under RCP 8.5. We hold the within-month realization of weather used to construct each daily projection fixed at w_0. We hold the empirical quantile k fixed at the median value.

- Within-month weather uncertainty, $Var(I^{mwk}|m = m_0, k = 50)$, from 10 realizations of within-month weather w. We set the fixed climate realization m_0 to the HadGEM-AO GCM model, as it recovers scenario that is "near median" by many measures (discussed below). We hold the empirical quantile k fixed at the median value.

- Econometric uncertainty, $Var(I^{mwk}|m = m_0, w = w_0)$, from 25 draws of econometric uncertainty by varying k systematically. We set the fixed climate realization m_0 to the HadGEM-AO GCM model and the weather used to construct each daily projection fixed at w_0.

- Total uncertainty, $Var(I^{mwk})$, from 11000 impact estimates where we resample from all GCMs, within-month weather realizations, and draws from the distribution of econometric results.

The interaction term Λ is computed as a residual. These values are computed for each sector and many subsectors, displayed in Figure S6 for end of century uncertainty, as a fraction of baseline damages. The evolution of the fractions of total variance driven by climate, weather, econometric uncertainty, and λ in projections over the century is shown in Figure S7, following the same approach as in ref. (*43*).

Below we derive the form of Λ and also check that it correctly relates to values recovered in each sector in Section F.2. We also explore how these results change if we select a different climate realization as the benchmark m_0.

F.1 Analytical derivation of Λ

To see why Λ has the magnitudes and signs we display in Figure S6, we consider a simplified model where an outcome Y is a function of mean temperature T. A single parameter A characterizes the structure of the econometrically derived dose-response function. A and T are independent random variables. We compute $Y = f(A, T)$, and wish to understand $Var(Y)$ as a function of the distribution of the random variables A and T. To do so, we derive the relationships between the following quantities

- $Var(Y|A = A_0)$, the climate-driven uncertainty
- $Var(Y|T = T_0)$, the econometric-driven uncertainty
- $Var(Y)$, the total uncertainty

where the interaction term Λ is defined as

$$\Lambda = Var(Y) - Var(Y|A = A_0) - Var(Y|T = T_0).$$

F.1.1 The linear case

Let $Y = \alpha + \beta A + \gamma T$. Then

$$\begin{aligned} Var(Y) &= \beta^2 Var(A) + \gamma^2 Var(T) \\ Var(Y|A = A_0) &= \gamma^2 Var(T) \\ Var(Y|T = T_0) &= \beta^2 Var(A) \\ \Lambda &= 0 \end{aligned}$$

For this linear case, this result is invariant to the choice of T_0 and A_0. This would imply that in this case of our actual calculations, the variances will not depend on the choice of GCP used as m_0.

F.1.2 The multiplicative case

Let $Y = AT$, as would be the case for a regressed linear relationship between temperature and an outcome, with an estimated coefficient A. In this multiplicative case, interacting uncertainty causes the total variance to differ from the sum of individual uncertainties, and the variance attributable to individual uncertainties differs depending on the A_0 and T_0.

$$\begin{aligned} Var(Y) &= E(A)^2 Var(T) + E(T)^2 Var(A) + Var(A)Var(T) \\ Var(Y|A = A_0) &= A_0^2 Var(T) \\ Var(Y|T = T_0) &= T_0^2 Var(A) \end{aligned}$$

So the interaction term is

$$\begin{aligned} \Lambda &= E(A)^2 Var(T) + E(T)^2 Var(A) + Var(A)Var(T) - A_0^2 Var(T) - T_0^2 Var(A) \\ &= Var(A)Var(T) + \left(E(A)^2 - A_0^2\right) Var(T) + \left(E(T)^2 - T_0^2\right) Var(A) \end{aligned}$$

If $A_0 = E(A)$ and $T_0 = E(T)$, then

$$\Lambda = Var(A)Var(T)$$

which is always positive. Note that this interaction term is distinct from the covariance of A and T, which is assumed 0.

F.1.3 Nonlinear functions of climate variables

Let $Y = Af(T)$. We derive a general approximation to the variance under any function, show that the sign of the interaction is negative for sufficiently concave functions, and quantify this relationship in the special case where $f(T) = T^{\alpha}$.

First, we apply a transformation of variables, under a Taylor approximation,

$$\begin{aligned} E(f(T)) &\approx f(E(T)) + \frac{f''(E(T))}{2} Var(T) \\ Var(f(T)) &\approx f'(E(T))^2 Var(T) \end{aligned}$$

We can then substitute these expressions into the variance of terms for the multiplicative case above

$$\begin{aligned} Var(Y) \approx & E(A)^2 f'(E(T))^2 Var(T) + \\ & \left(f(E(T)) + \frac{f''(E(T))}{2} Var(T) \right)^2 Var(A) + Var(A) f'(E(T))^2 Var(T) \\ Var(Y|A = A_0) \approx & A_0^2 f'(E(T))^2 Var(T) \\ Var(Y|T = T_0) \approx & f(E(T))^2 Var(A) \end{aligned}$$

Let $A_0 = E(A)$ and $T_0 = E(T)$. Then the interaction term is

$$\begin{aligned} \Lambda &= \left(2f(E(T)) \frac{f''(E(T))}{2} Var(T) + \left(\frac{f''(E(T))}{2} Var(T) \right)^2 \right) Var(A) + Var(A) f'(E(T))^2 Var(T) \\ &= Var(A)Var(T) \left(f'(E(T))^2 + f(E(T)) f''(E(T)) + \frac{f''(E(T))^2}{2} Var(T) \right) \end{aligned}$$

Note that the first and third terms are necessarily positive, and the sign of the second term depends on the degree of concavity.

Overall, we are interested in the sign of Λ across possible values of α. Consider the case of $f(T) = T^{\alpha}$, so that $f'(E(T)) = \alpha E(T)^{\alpha-1}$ and $f''(E(T)) = \alpha(\alpha-1)E(T)^{\alpha-2}$. The interaction term would then be

$$\Lambda = Var(A)Var(T)\left((\alpha E(T)^{\alpha-1})^2 + \alpha(\alpha-1)E(T)^{\alpha}E(T)^{\alpha-2} + \frac{(\alpha(\alpha-1)E(T)^{\alpha-2})^2}{2}Var(T)\right)$$

Note that the second term is negative if $0 < \alpha < 1$ and that for any value of $\alpha > 1$ (representing a high level of convexity) than it must be true that $\Lambda > 0$. For $\alpha < 0$, then $\Lambda > 0$. To find the value of $0 < \alpha < 1$ for which Λ is negative, we can set $\Lambda = 0$ and solve for α. We therefore look for a solution to the cubic equation in α:

$$\alpha^2 E(T)^{2\alpha-2} + \frac{\alpha^2(\alpha-1)^2 E(T)^{2\alpha-4}}{2}Var(T) = -\alpha(\alpha-1)E(T)^{2\alpha-2}$$

If $E(T)^2$ is large, the solution for α is approximately 0.5. Thus, for values of α roughly greater than 0.5 then $\Lambda > 0$ and for α roughly less than 0.5 then $\Lambda < 0$. Therefore, an impact function of the form $f(T) = T^{\alpha}$ must be at last as concave as a square root function to produce a negative interaction term.

F.2 Relationship between cases and sectors

Here, we relate the response functions in Figure S4 (some of which are displayed in Figure 1 in the main text) to the derivations above.

The response to CO_2 fertilization corresponds to the linear case, since uncertainty in the estimated effect of CO_2 does not interact with uncertainty in the projected concentration of CO_2, which is assumed known in each scenario.

The response curve that most closely matches the multiplicative case is violent crime, which shows a nearly uniformly increasing response in temperature. Violent crime shows a small, positive interaction term, as predicted.

For the other impacts, we find negative interaction terms for agriculture, labor, and property crime,

and positive interaction terms for mortality. These correspond to the shapes of the curves, with agriculture, labor, and property crime describing concave functions across temperature, and mortality following a convex curve.

G Energy impact modeling

To assess the impact of changes in temperature on energy demand and expenditures, we use RHG-NEMS, a version of the Energy Information Administration's (EIA) National Energy Modeling System (NEMS) (*31*), maintained by the Rhodium Group. RHG-NEMS is a detailed multi-sector bottom-up model of US energy supply and demand with detailed residential, commercial, and industrial demand modules, electricity and primary energy supply modules, and energy market and macroeconomic modules, among others. Consumer demand is derived from detailed consumer choice algorithms that allow consumers to substitute, subject to limited foresight, from a wide array of available end-use technologies in order to satisfy their energy service demands (see Section G.2).

In this study, NEMS is used to develop response functions relating climate variables to changes in the energy system. Specifically, we project changes in residential and commercial electricity demand, residential and commercial total energy expenditures, and electricity generating capacity. The response functions are derived from the outputs of NEMS in 2040 under a range of temperature scenarios. These responses are then mapped to county-level changes in climate variables in each time period (2020-2039, 2040-2059, and 2080-2099).

G.1 Physical Data

We model changes in energy demand by varying the number of heating degree days (HDDs) and cooling degree days (CDDs), which in turn drive heating and cooling service requirements in NEMS. HDDs and CDDs are a measure of the approximate number of degrees that a living space must be heated or cooled for each day summed over all the days in the year. Daily minimum and maximum temperature projections were drawn from the outputs of the climate modeling process (*19*), meaning that the projections are both consistent with the other impact categories in this study, and that they covary in the macroeconomic

modeling process. The method for calculating HDDs and CDDs is described in Tables S2 and S3 (see for example (*78*)).

Supplementary Table S2: Formula for calculating daily HDD-65

Condition	**Formula Used**
$T_{min} > 65F$	$D_h = 0$
$T_{min} \leq 65F$ and $\frac{(T_{max}+T_{min})}{2} > 65F$	$D_h = \frac{(65F-T_{min})}{4}$
$T_{max} \geq 65F$ and $\frac{(T_{max}+T_{min})}{2} \leq 65F$	$D_h = \frac{(65F-T_{min})}{2} - \frac{(T_{max}-65F)}{4}$
$T_{max} < 65F$	$D_h = 65F - \frac{(T_{max}+T_{min})}{2}$

Supplementary Table S3: Formula for calculating daily CDD-65

Condition	**Formula Used**
$T_{max} < 65F$	$D_c = 0$
$T_{max} \geq 65F$ and $\frac{(T_{max}+T_{min})}{2} < 65F$	$D_c = \frac{(T_{max}-65F)}{4}$
$T_{min} \leq 65F$ and $\frac{(T_{max}+T_{min})}{2} \geq 65F$	$D_c = \frac{(T_{max}-65F)}{2} - \frac{(65F-T_{min})}{4}$
$T_{min} > 65F$	$D_c = \frac{(T_{max}+T_{min})}{2} - 65F$

G.2 RHG-NEMS

Our analysis of the impact on residential and commercial heating and cooling demand due to climate change relies heavily on RHG-NEMS, a version of the Energy Information Administration's (EIA) National Energy Modeling System (NEMS) maintained by the Rhodium Group. EIA uses NEMS to produce their Annual Energy Outlook (AEO), which projects the production, conversion, consumption, trade, and price of energy in United States through 2040. NEMS is an energy-economic model that combines a detailed representation of the US energy sector with a macroeconomic model provided by IHS Global Insight. The version of RHG-NEMS used for this analysis is keyed to the 2013 version of the AEO. The NEMS model is documented in full in (*31*). Documentation of the macroeconomic and energy sector assumptions used in the AEO 2013 version of NEMS is available in (*62*).

RHG-NEMS is designed as a modular system with a module for each major source of energy supply, conversion activity and demand sector, as well as the international energy market and the US economy (Figure S8). The integrating module acts as a control panel, executing other RHG-NEMS modules to ensure energy market equilibrium in each projection year. The solution methodology of the modeling

system is based on the Gauss-Seidel algorithm. Under this approach, the model starts with an initial solution, energy quantities and prices, and then iteratively goes through each of the activated modules to arrive at a new solution. That solution becomes the new starting point and the above process repeats itself. The cycle repeats until the new solution is within the user-defined tolerance of the previous solution. Then the model has 'converged', producing the final output.

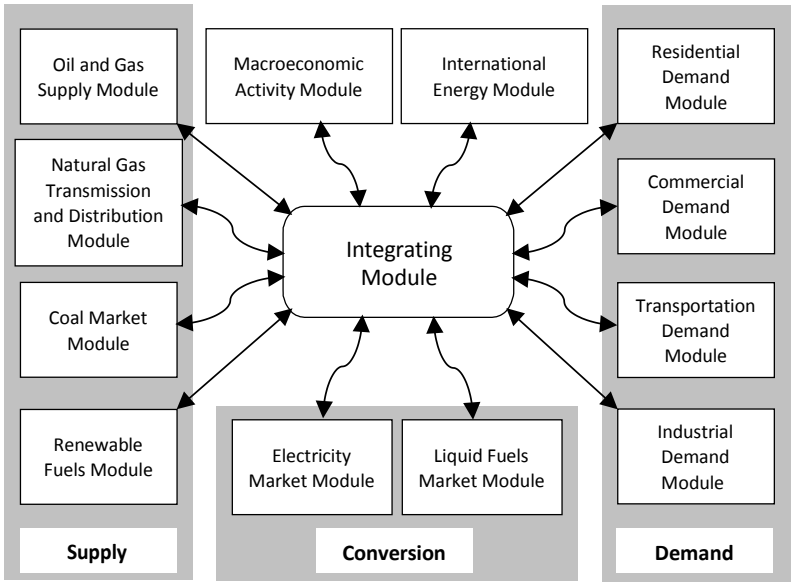

Supplementary Figure S8: Basic NEMS structure and Information Flow

G.2.1 Residential and commercial demand modules

Index Value	Census Division	Housing Type	Fuel	Technology Choice
1	New England	Single Family	Distillate	Space Heating
2	Middle Atlantic	Multifamily	LPG	Space Cooling
3	East North Central	Mobile Home	Natural Gas	Clothes Washing
4	West North Central		Electricity	Dishwashing
5	South Atlantic		Kerosene	Water Heating
6	East South Central		Wood	Cooking
7	West South Central		Geothermal	Clothes Drying
8	Mountain		Coal	Refrigeration
9	Pacific		Solar	Freezing

Supplementary Table S4: Residential Module: Key Variables

In RHG-NEMS, energy consumption estimates of residential and commercial sectors are modeled using the Residential and Commercial Demand modules. The Residential Demand Module projects energy

Index Value	Census Division	Building Type	Fuel	End-use Service
1	New England	Assembly	Electricity	Space Heating
2	Middle Atlantic	Education	Natural Gas	Space Cooling
3	East North Central	Food Sales	Distillate Oil	Water Heating
4	West North Central	Food Service	Residual Oil	Ventilation
5	South Atlantic	Health Care	LPG	Cooking
6	East South Central	Lodging	Steam Coal	Lighting
7	West South Central	Office - Large	Motor Gasoline	Refrigeration
8	Mountain	Office - Small	Kerosene	Office Equip. - PCs
9	Pacific	Mercantile & service	Wood	Office Equip. - other
10		Warehouse	Municipal Solid Waste	Misc. End-Use Loads
11	U.S. Total	Other	Hydro	
12			Waste Hear	
13			Other Gaseous Fuels	

Supplementary Table S5: Commercial Module: Key Variables

Supplementary Table S6: Predicted change in residential and commercial electricity demand from a change in 1 Heating Degree Day (HDD) / Cooling Degree Day (CDD)

Census Region	HDD	CDD
New England	0.00056%	0.00329%
Middle Atlantic	0.00150%	0.00895%
East North Central	0.00101%	0.00924%
West North Central	0.00023%	0.00755%
South Atlantic	0.00040%	0.00718%
East South Central	-0.00138%	0.00620%
West South Central	-0.00047%	0.00742%
Mountain	0.00061%	0.00881%
Pacific	0.00130%	0.00673%

demand by end-use service, fuel type, and Census division (Table S4). Similarly, the Commercial Demand Module projects energy demand by end-use service and fuel type for eleven different categories of buildings in each Census division (Table S5). Both modules use energy prices and macroeconomic projections from the RHG-NEMS system to estimate energy demand based on extensive exogenous inputs including consumer behavior, appliance efficiency and choices, and government policies.

One of the factors affecting energy demand in RHG-NEMS is climate. Future climate is represented as annual HDDs and CDDs by census region in both the residential and commercial demand modules. The modules incorporate the future change in heating demand (due to change in HDDs) and cooling demand (due to change in CDDs) to inform decisions about appliance purchases as well as total energy

Supplementary Table S7: Predicted change in residential energy expenditures from a change in 1 Heating Degree Day (HDD) / Cooling Degree Day (CDD)

Census Region	HDD	CDD
New England	0.000045%	0.000117%
Middle Atlantic	0.000045%	0.000150%
East North Central	0.000043%	0.000165%
West North Central	0.000036%	0.000224%
South Atlantic	0.000089%	0.000179%
East South Central	0.000070%	0.000188%
West South Central	0.000169%	0.000178%
Mountain	0.000014%	0.000223%
Pacific	0.000062%	0.000170%

Supplementary Table S8: Predicted change in commercial energy expenditures from a change in 1 Heating Degree Day (HDD) / Cooling Degree Day (CDD)

Census Region	HDD	CDD
New England	0.000045%	0.000180%
Middle Atlantic	0.000036%	0.000138%
East North Central	0.000030%	0.000130%
West North Central	0.000052%	0.000132%
South Atlantic	0.000095%	0.000140%
East South Central	0.000076%	0.000110%
West South Central	0.000175%	0.000147%
Mountain	0.000027%	0.000111%
Pacific	0.000031%	0.000137%

consumption. For further details see Residential Demand module (*79*) and Commercial Demand module documentations (*80*).

G.3 Impact Estimation

Due to the complexity and run time of RHG-NEMS, running the model for each of our daily projections was infeasible. Instead, we constructed representative scenarios that systematically varied the HDDs and CDDs from our baseline and recorded the response of the model in the variables of interest: changes in energy and electricity demand, energy and electricity expenditures and electricity generation capacity. Using the results of these runs, we built the response functions to estimate, for each census region, the percent change in a particular variable due to absolute changes in the number of HDDs and CDDs. Tables S6, S7, S8, and S9 show the predicted change in electricity demand, residential energy consumption,

Supplementary Table S9: Predicted change in national electricity capacity required from a change in 1 Heating Degree Day (HDD) / Cooling Degree Day (CDD)

	HDD	**CDD**
US Total	0.08184 GW	0.2856 GW

commercial energy consumption, and national capacity, respectively, from an increase in 1 HDD or CDD.

The relative changes in electricity demand, residential energy consumption, commercial energy consumption, and capacity were estimated using a Monte Carlo simulation using the projections of county daily temperature extremes. The HDD-CDD response functions given above are applied to all counties within each census region. This process yields sets of correlated estimates of percent changes in electricity demand, and energy expenditures at the county level for each year in the analysis. Changes in state, regional, and national quantities use population-weighted average responses. State-level absolute changes in electricity demand (in kWh) and energy expenditures (in 2012 USD) were estimated at the state level using EIA estimates of state electricity sales (*63*) and energy expenditures (*81*).

H Coastal impact calculations

Coastal impacts are calculated using modified versions of RMS's catastrophe loss models for North Atlantic Hurricane & Storm Surges and U.S. Winter Storms. These models are run with RMS's proprietary database of property exposure for all 21 coastal states of the continental United States and the District of Columbia.

Catastrophe models are designed to provide synthetic catalogues of extreme events representing hundreds of thousands of years of activity, rather than the typically less than a hundred years of historical observations available, thereby reducing the dependence on limited historical experience for calculating risks. These stochastic catalogues are derived from a combination of statistical and physics-based models, ensuring that the catalogues are composed of physically realistic events while also extending the historical experience to encompass a fuller range of physically possible scenarios.

RMS models and data are proprietary and are not formally documented in the scientific peer-reviewed literature. However, as an established part of how insurers and reinsurers manage their business, catas-

trophe models are subject to significant regulatory review (e.g., the Florida Commission on Hurricane Loss Projection Methodology, https://www.sbafla.com/method/) as well as independent evaluation by the model users in the (re)insurance community, many of whom maintain dedicated teams of scientists to evaluate commercial models. For a model to be accepted, it must be able to both replicate the actual losses experienced in recent events and show that the loss exceedance probability distribution, at shorter return periods, is consistent with the past few decades of loss experience.

H.1 Structure of a catastrophe model

The structure of catastrophe models involves four related but independently validated and calibrated components: hazard, exposure, vulnerability, and loss.

The hazard component characterizes the frequency, intensity, and spatial distribution of a peril. It may also include secondary perils, such as storm surge in the case of tropical cyclones.

The exposure component quantifies the people or property exposed to a hazard and is the primary user-defined input into catastrophe model software. RMS also maintains a database of 'industry' exposure that captures the location, value, and primary characteristics (e.g. residential versus commercial or industrial usage) of all property at a zip-code resolution throughout the United States.

The vulnerability component accounts for the response of the exposure to the hazard. For property exposures, vulnerability functions estimate the damage to structures and their contents that result from a given hazard level, as well as the amount of time required for rebuilding, additional living expenses and business interruption costs.

The loss component estimates the impacts – most often monetary costs of property damage – produced by the combination of hazard, exposure, and vulnerability, as well as secondary impacts that can amplify losses, such as the increasing cost of labor due to the economic demand surge following a major catastrophe.

H.2 Hurricane and storm surge modelling

The RMS North Atlantic Hurricane Model uses a stochastic event set to estimate direct damage and losses from wind and storm surges. A parametric, time-stepping wind field model is used and accounts

for surface characteristics and upstream roughness. The storm surge hazard model uses wind and pressure fields from the stochastic event set as forcing (i.e., as input) to the MIKE 21 hydrodynamic model system (*33*) to estimate still-water (i.e., without wave effects) storm surge elevations. The hurricane wind model is calibrated to insurance claims data and as such implicitly includes related damage from treefall, wind missiles, rain infiltration, etc. The storm surge loss model is likewise calibrated against actual flooding loss experience. The model does not include the following potential sources of loss: inland flooding from hurricane-related rainfall (including the contribution this may have on storm surge levels); chaotic localized weather systems within the hurricane circulation, such as tornadoes and hailstorms; losses from any source occurring in areas that experience wind speeds below a modeling threshold of 50 mph (80 km/h); and contingent and other indirect time-element coverages (i.e., contingent business interruption). Furthermore, the RMS North Atlantic Hurricane Model only includes storms that affect land at hurricane strength (i.e., Category 1 or greater), and tropical storms that never reach hurricane strength or that fall below hurricane strength far from land are not included in the model.

H.2.1 Stochastic event set

The stochastic event set consists of thousands of simulated storm tracks representing more than 100,000 years of hurricane activity. The event set is generated using a statistical track model (*34*) that extrapolates the HURDAT catalogue (*82*) to generate simulated tracks having similar statistical characteristics to the HURDAT historical tracks. Stochastic tracks are simulated from genesis (starting point) to lysis (last point) and provide the key drivers of risk, including landfall intensity, landfall frequency, and landfall correlation.

The frequency of events is calibrated to ensure that simulated landfall frequencies agree with the historical record. Target landfall rates are computed on a set of linear coastal segments ('RMS gates') by smoothing the historical landfall rates. The RMS smoothing technique uses long coastal segments, obtained by extending each RMS gate in both directions and keeping the orientation constant. Historical storms that cross an extended gate contribute to the landfall rate at the corresponding original segment.

Importance sampling of the simulated tracks is performed to create the computationally efficient event set used for loss cost determinations. Each of these events has a frequency of occurrence given by its

mean Poisson rate based on the calibration of historical event frequencies (HURDAT 1900–2011).

H.2.2 Wind Hazard Module

The wind hazard module generates wind fields from both landfalling hurricanes and bypassing storms. Once tracks and intensities have been simulated by the stochastic module, the wind field module simulates 10-meter, three-second gusts, accounting for upstream surface roughness and local effects, output onto a variable resolution grid ranging from 1km to 10km. The size and shape of the time stepping wind fields are generated using an analytical wind profile derived from (*32*). Peak gusts are used rather than sustained wind speed, as they are the best determinant of building damage and are used as the basis of many building codes world-wide, including the U.S.

H.2.3 Wind Vulnerability Module

The wind vulnerability module relates the expected amount of physical damage to buildings and contents to the modeled peak three-second gust wind speed at that location. The severity of the damage is expressed in terms of a mean damage ratio (MDR), which is defined as the ratio of the expected cost to repair the damaged property relative to its overall replacement cost. The wind vulnerability module also estimates the variability in the expected damage ratio and models it with a beta distribution. Time-element losses due to business interruption and additional living expenses are estimated using occupancy-dependent facility restoration functions that relate the expected duration of the loss of use to the modeled building damage.

H.2.4 Storm Surge Hazard Module

Storm surge in the numerical model is driven by the wind stress from the time-stepping wind field and the influence of the cyclone's low-pressure field, as well as the influence of tides. The storm surge is dependent on the storm's characteristics before landfall, with a large storm surge resulting from the accumulated impact of the inverse barometric effect and wind stress acting for many days before the storm nears the coast. Storms may weaken close to landfall but still retain much of the surge associated with their offshore intensity. For example, because Hurricane Katrina, reached Category 5 intensity in

the Gulf of Mexico even while it had weakened to Category 3 at landfall, it still produced a powerful 27-foot (8.3 m) surge on the Mississippi coast.

In urban coastal areas, the resolution of the surge footprint is 100m. This resolution decreases to 500m in non-urban areas, and 10km in very flat areas. The elevation of the terrain at the specified location is then subtracted from the surge height to derive the depth of flooding. Once the elevation is subtracted from the surge height at a location, the wave height is calculated based on the depth of flooding and the velocity of the flow. The velocity of the flow is dependent on the proximity to the open sea and local convergence in the flow due to topography. For elevated buildings that meet the construction class and year built criteria and are within a FEMA "100-year flood zone", the Base Flood Elevation is applied to calculate an effective flood depth. RMS has implemented improved elevation data based on the USGS National Elevation Dataset (NED), enhanced with airborne LIDAR data where available, and stored on an underlying 100m uniform resolution grid.

H.2.5 Storm Surge Vulnerability Module

The storm surge vulnerability module relates the expected amount of physical damage to buildings and contents to the modeled storm surge flood depth, including the effects of wave action, if present. Like the wind vulnerability module, the severity of the damage is expressed in terms of a mean damage ratio (MDR), and the variability in the damage is characterized by a beta probability distribution. The storm surge vulnerability functions for buildings and contents are derived from a database of flood-related damage observations compiled by the U.S. Army Corps of Engineers (USACE) from major flood events in the U.S. This database consists of flood/depth/damage ratio relationships that relate the incurred flood-related loss to the observed flood depth for different occupancy types. The storm surge vulnerability functions also incorporate structural-engineering-based adjustments to account for the effects of the building height and construction class on the expected damage and are calibrated and validated using claims data from multiple storms.

Two sets of storm surge vulnerability functions are employed so as to differentiate between locations exposed to low velocity flooding only and locations potentially exposed to significant wave action. The low-velocity flooding curves, which are referred to as surge vulnerability functions, relate the MDR of a

building or its contents to the estimated flood depth according to its occupancy type, construction class and number of stories. The wave vulnerability functions are used for loss calculations when a location has been characterized as unsheltered and the water depth exceeds seven feet. For a given building type and surge depth, the damage ratio predicted by the wave vulnerability function can be much higher than that predicted by the corresponding low-velocity surge vulnerability function, reflecting the additional damaging energy imparted by the wave action.

H.2.6 Accounting for climate change

RMS models are designed to represent the "current" risks due to climate-related natural catastrophes, as the users of these models are primarily insurers and reinsurers writing one year contracts. For the purposes of this study, adjustments have been made to account for expected changes in climate conditions. Local sea-level rise projections (*36*) are incorporated by adjusting the base water heights in the Storm Surge Hazard Module. Changes in hurricane frequency and intensity (*35, 65*) have been incorporated by adjusting the "Stochastic Event Module", specifically the frequency of occurrence of each event in the event set. For the purposes of this analysis, many hundred alternative versions of the model were created to span the range of time periods, RCPs, and sea-level rise projections, as well as alternative projections of changes in hurricane frequency and intensity.

Local sea-level rise projections. A reduced set of state-specific sea-level rise projections for coastal states is derived from the local sea-level rise projections of ref. (*36*). The flood damages are assumed to be path independent. For each state, 22 relative sea levels are taken to span the range from 0 cm to the 99.9th percentile of pooled RCP 2.6, 4.5 and 8.5 projections, based on the time series of median projections from 2000 and 2100 and the 0.5th to 99.9th percentile range for 2100. The "Storm Surge Hazard Model" calculates the local inundation water heights of each stochastic event on 18 local grids nested within a lower resolution regional grid covering the domain of the model. The reduced sea-level projections is mapped to the individual local grids to assign each grid a specific increase in sea level. The surge height of the footprint of each event is then adjusted at this local level before being recombined into a coherent 'event' footprint (which can cover multiple local grids).

From this reduced set of projections, we develop for each state a set of curves describing the rela-

tionship between local sea-level (LSL) rise and expected annual damages (Figure S9). These impacts are aggregated nationally and indexed against global MSL rise to construct Figure 4F.

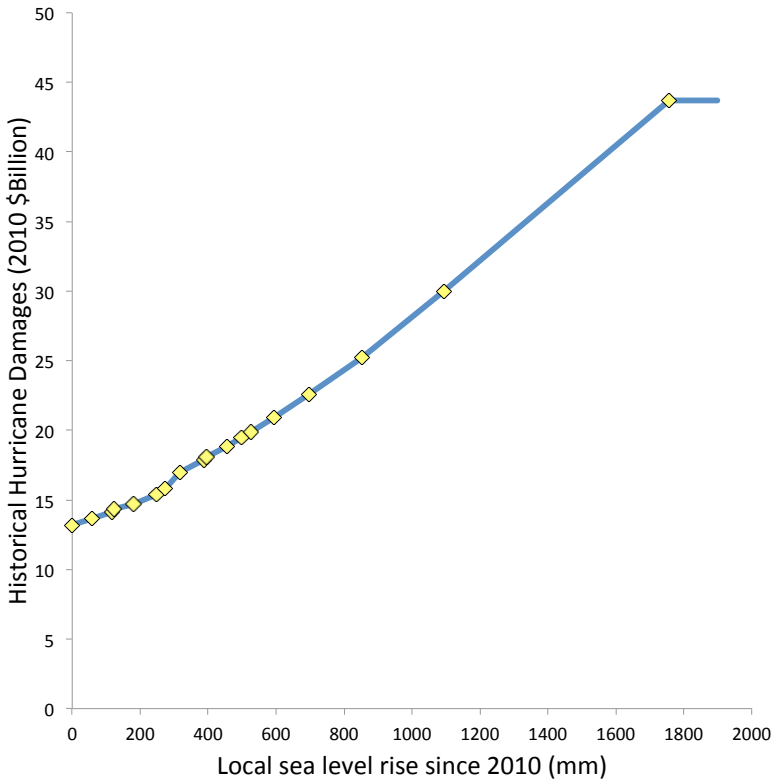

Supplementary Figure S9: **Sample damage function relating local sea level (LSL) to annual coastal storm damages in Florida**. RMS estimates (yellow) are linearly interpolated to form a damage function (blue). The function is constrained to be monotonically increasing in LSL, and is held constant past the highest LSL estimate provided. Using this method, damage estimates from the RMS Model are used to parameterize functions modeling property below sea level, direct storm damage, and business interruption impacts separately for coastal and inland areas in each state in the RMS exposure dataset.

For each RCP and each state, this damage curve is combined with the full set of probabilistic projections of (*36*) to generate state-level probability distributions for the change in coastal storm damages due to sea-level rise.

Changes in hurricane frequency and intensity. For RCP 4.5, Knutson et al. (*65*) projected future hurricane activity in the Atlantic basin by downscaling the CMIP5 ensemble mean. These changes were mapped directly to the "RMS historical rate set" according to the maximum lifetime intensity category of each storm in the event set. Knutson et al. provide the relevant changes by storm intensity category for early- and late-twenty-first century time-slices, from which linear interpolation / extrapolation was used

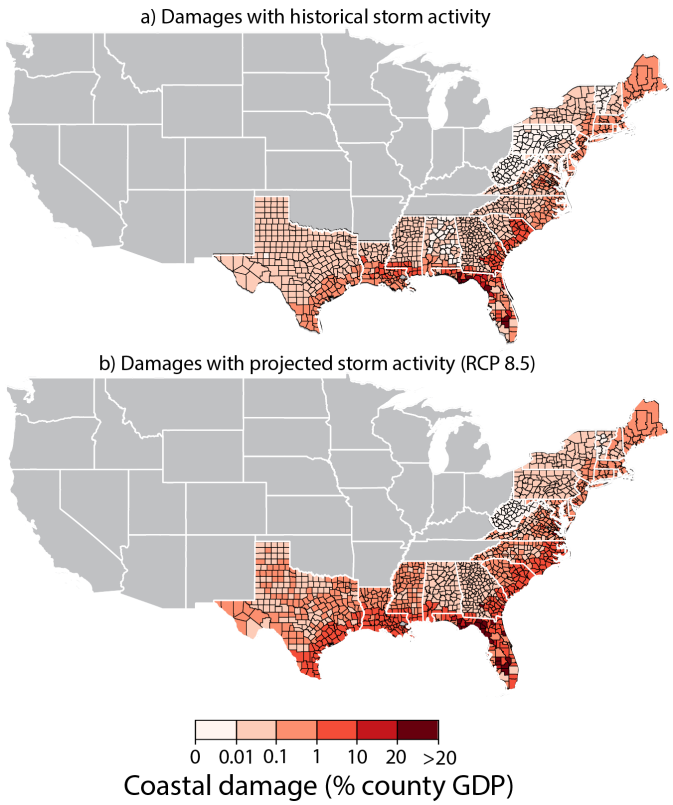

Supplementary Figure S10: **Comparing damages with and without cyclone intensification.**. (A) Same as Figure 2F in the main text. (B) Same, but using projected cyclone activity for RCP8.5.

to infer the changes over the course of the century.

For RCP 8.5, Emanuel (*35*) (supplemented through personal communications) downscaled 6 individual GCMs from CMIP5. These results were obtained as absolute values for basin activity and for activity at landfall (across the entire north Atlantic domain) by maximum storm intensity (as measured by the maximum 1-min sustained wind speed). Projections were provided for current, mid- and late-twenty-first century time-horizons. The difference between the future and current activity is used to define a percentage change in activity and linear interpolation / extrapolation is used to infer the percentage changes at the over the course of the century. Ensemble-mean changes were applied directly to the "RMS historical rate set" according to the maximum lifetime intensity or maximum landfall intensity of each storm in the event set to create multiple alternative rate sets. The effect of projecting storm activity on the distribution of damages in shown in Figure S10. Projected storm activity was not included in the construction of damage functions because there was no variation in GMST across simulation runs and projected activity was only available for RCP8.5.

H.3 Winter Storm Modelling

The RMS U.S. Winter Storm Model follows the same basic structure as the Hurricane model, using a stochastic event set to estimate direct damage and losses from wind, ice load, snow and freeze.

The winter storm stochastic event set is designed to model the full variation in winter storm risk by simulating the complex spatial patterns of the winter storm perils and their interdependency using a hybrid modeling approach. The large-scale stochastic winter storm events and their corresponding tracks are simulated using the Community Atmospheric Model (CAM) 3.0 (*83*), run at approximately 250 km resolution. The resulting tracks are calibrated based on statistical modeling of historical winter storm track observations. The CAM stochastic event set is then downscaled using the high-resolution numerical weather prediction MM5 model (*84*) and further calibrated using daily and hourly meteorological observations of snow, precipitation, wind, and temperature.

Storm surges associated with low pressure system are not explicitly represented in the U.S. Winter Storm Model. To account for the effect of sea-level change on winter storm surge losses, a relationship between the observed surge levels and modeled surge losses during historical hurricanes was used to estimate an expected winter storm surge loss based on observed surge levels during winter storms. We assumed that the ratio between the average annual surge loss for hurricanes (assuming no change in storm frequency or intensity) and the average annual surge loss for winter storms will remain constant as sea levels rise. Based on this assumption, and with the direct calculation of the changes in hurricane storm surge losses, we generate expected increases in average annual surge loss from winter storms.

I Valuation of direct damages by sector

In order to aggregate over each individual sector to obtain a total economic response to climate forcing, we first apply a monetary valuation to each individual sector. The valuation for specific sectors is discussed below. For all direct damages, values are held at constant prices and presented as a proportion of US Gross Domestic Product. As such, the relative weighting of each sector remains the same as the 2011 economy and, by being expressed as a percentage change, would scale with the expansion of the economy while holding the structure of the economy fixed. There are no general equilibrium adjustments

made to sectors for assessment of direct damages, although prices and factor intensities are adjusted in the CGE exercise. Valuations are employed at two spatial resolutions:

1. National level average values are applied for calculations in Figures 5A-B. Aggregation to a national level impact is performed as described in Section E.

2. County level valuation is used for calculations in Figure 5C.

I.1 Agriculture

To value the direct costs and benefits from changes in production quantity, we assume that a given change in agricultural output results in a proportional change in the value of that sector's gross output in the reference year. The value of impact sector gross output in a given state and year was calculated as the portion of all agriculture output made up by the impacted crop in a given region in the IMPLAN dataset (*66*) times national gross output given by BEA (*85*). The potential for crop switching or land use change was not accounted for in calculating direct costs and benefits; instead, areas that experienced changes in productivity, either positive or negative, had that productivity applied to the existing production in that area. The total cost for all agriculture was found by summing the impacts from the component crops.

I.2 Crime

Crime impacts are valued using the method described in (*38*). Changes in property and violent crime are multiplied by current crime levels using the FBI's "Crime in the United States" dataset (*86*), and the cost estimates, given in 2007 USD, are adjusted to 2011 USD using the BEA national real GDP deflator.

I.3 Coastal Damages

Coastal impacts were derived directly from the process modeling method described in Section H. The total costs of climate damages includes climate-driven changes in average annual loss from tropical cyclones and other coastal storms—either induced by higher local sea level interacting with storms and/or greater storm frequency—averaged over 20-year periods. Losses from permanent inundation were omitted from our accounting because the spatial covariance before future economic growth, adaptive behavior,

and exposure to MSL rise is known to be exceptionally high (*87*), invalidating the basic assumptions of our analysis.

I.4 Energy

The direct costs and benefits of climate-driven changes in energy demand were assessed using RHG-NEMS, a version of the National Energy Modeling System (NEMS), developed by the EIA (*31*) for use in the Annual Energy Outlook (see, for example, (*62*)) and maintained by the Rhodium Group. A detailed description of those methods is given in Section G.

I.5 Labor

To calculate the direct costs and benefits, we assume that the direct effect of a climate-driven labor productivity change is equal to state-level estimates of value added by labor (*88*), distributed among high-and low-risk sectors using IMPLAN data (*66*), times the change in labor productivity at the county level.

I.6 Mortality

To value mortality, we follow the US Environmental Protection Agency (EPA) in applying the value of a statistical life (VSL) of $7.9 million (in 2011$) as a benchmark estimate of Americans' "willingness-to-pay" to reduce mortality risk. This includes both market and non-market costs.

J Damage function calculation

J.1 Sectoral national-level damage functions

Constructing sectoral damage functions requires that losses in each sector are represented as conditional on global mean surface temperature (GMST) change. To do this for each RCP r by climate realization m tuple, we calculate $\Delta GMST^{rm}$, the change in GMST averaged between 2080 and 2099 relative to the baseline. This results in 116 values of $\Delta GMST^{rm}$. For each state of the world, county level annual

impacts I_{jt}^{rmwk} are calculated as in Section D, aggregated to the national level J as in Section E, and averaged over the years 2080-2099. For each sector, we collect the sets of impacts $I_{J,2080-2099}^{rmwk}$ and match them to the $\Delta GMST^{rm}$. Plotting impacts $I_{J,2080-2099}^{rmwk}$ against $\Delta GMST_{2080-2099}^{rm}$ gives us damages in a sector as a function of global climate change. These results are displayed in Figures 3 and S11-S13, with restricted cubic splines fit to the median, upper 90th percentile and lower 90th percentile of each state of the world $\{rm\}$. These results are not weighted because the likelihood of states of the world is not relevant to the description of the damage function. (As previously noted, sea level rise is not estimated as an explicit function of GMST and therefore cannot have a separate damage function.)

The restricted cubic splines in these figures are flexible summaries of damage functions described as conditional distributions, but they are somewhat more difficult to employ elsewhere. To simplify these damage functions, we also estimate polynomials that we find perform well at describing these relationships and are much easier describe analytically. Thus, we estimate summaries of these relationships by regressing the impact value (for all realizations) on 1st- through 4th-order polynomials of global mean surface temperature:

$$I_{J,2080-2099}^{rmwk} = \eta_0 + \sum_{\chi=1}^{\bar{\chi}} \eta_\chi \times (\Delta GMST_{2080-2099}^{rm})^\chi + \epsilon, \ \forall \, \bar{\chi} \in \{1, 2, 3, 4\} \tag{1}$$

Standard errors are clustered at the level of the climate realization m. Results of these regressions are shown in Tables S12–S11.

J.2 Aggregate national-level damage function

In order to compute the national level damage function (Figures 5A-B) we first calculate level changes for each projected year by using baseline values for each empirical sector (Section E). This gives us quantity changes in each sector. Applying the valuations described in section I, we obtain monetized changes for all sectors, resulting in a (non-normal) distribution of monetized impacts, which are then presented as a percentage of 2011 GDP. Within each RCP scenario r and climate realization m, we resample the distribution of sectoral impacts $I_{J,2080-2099}^{rmwk}$ 10,000 times and sum these draws from each distribution, which results in an aggregate national level empirical damage distribution for each $\Delta GMST_{2080-2099}^{rm}$. As sea level rise is independent of model temperature, we draw from the distribution of coastal damage

impacts within each RCP scenario and sum those draws to the empirical damage draws for each of the climate realizations within that RCP.

Following the same process as for the sectoral damage functions but for the sum of all sectoral impacts, we plot the aggregate national level damage function in Figure 5A, with quadratic fits for the upper 95th percentile and lower 5th percentile. Values for polynomials from 1st- to 4th-order are shown in Figure S14 with coefficients from regressions of the same form as equation 1 for total direct damages displayed in Table S16. We rely on the quadratic fit in the main text because it is essentially identical to the higher-order fits (Figure S14) but is more parsimonious. Values for the percentile bands are in Table S17.

As a verification exercise, in Figure S15 we re-estimate the national aggregate damage function using impacts and $\Delta GMST$ from 2040-2059 to compare against these 2080-2099 results. Many climate-economy models assume that the structure of damage functions do not vary over time, a hypothesis that this exercise fails to reject. The mid-century damage function covers a smaller range of $\Delta GMST$ because the range of projected warming across scenarios is narrower, but damages conditional on $\Delta GMST$ are not statistically different and credible intervals overlap substantially over the region of common support. Some difference is apparent—a balance between lower carbon fertilization in agriculture, lower storm damages from lower mean SLR, and differing spatial covariance between warming and the spatial distribution of populations and economic activity—although a single aggregate damage function appears to serve as a good approximation for projected conditional damages throughout the coming century.

J.3 Aggregating county-level damage functions

Figure S16 uses county-level data, and calculates adjustments to damages to account for risk and inequality of impacts. We note that valuations from Section I are not heterogenous across space, but county specific impacts vary as a function of heterogeneity in climate and in baseline levels in each sector across space. The process in calculating these impacts is identical to the previous section, except that we use non-aggregated county level data to obtain impacts $I^{rmwk}_{j,2080-2099}$ for each of 3,143 counties, indexed by j, to compute certainty-equivalent and risk-neutral damage functions (derived in Section K).

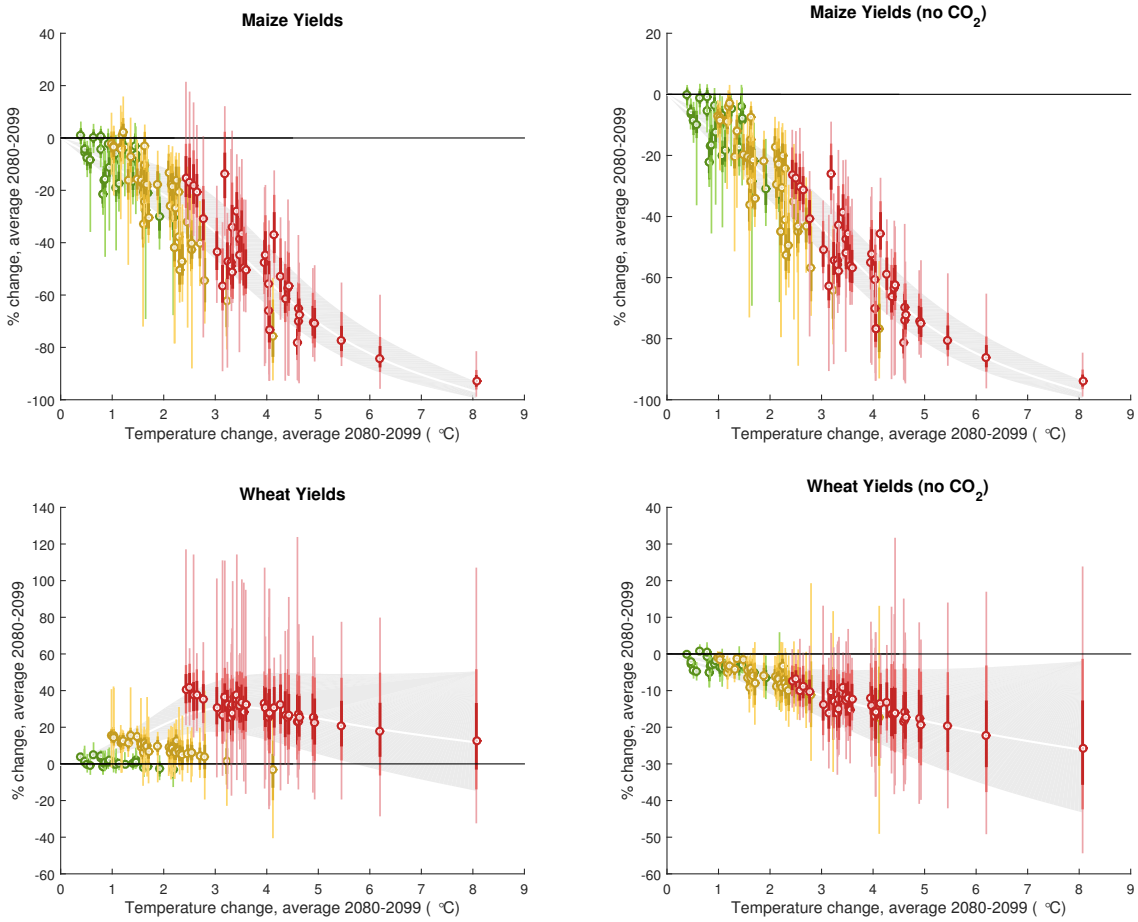

Supplementary Figure S11: **Agriculture damage functions by crop category.** Same as Figures 3A-B, but for maize and wheat only. Approximations to these response surfaces using polynomials, along with statistical uncertainty, are in Table S10. In the left column, discontinuous changes in average impacts and variances in impact between RCP scenarios are driven by the effects of CO2 fertilization.

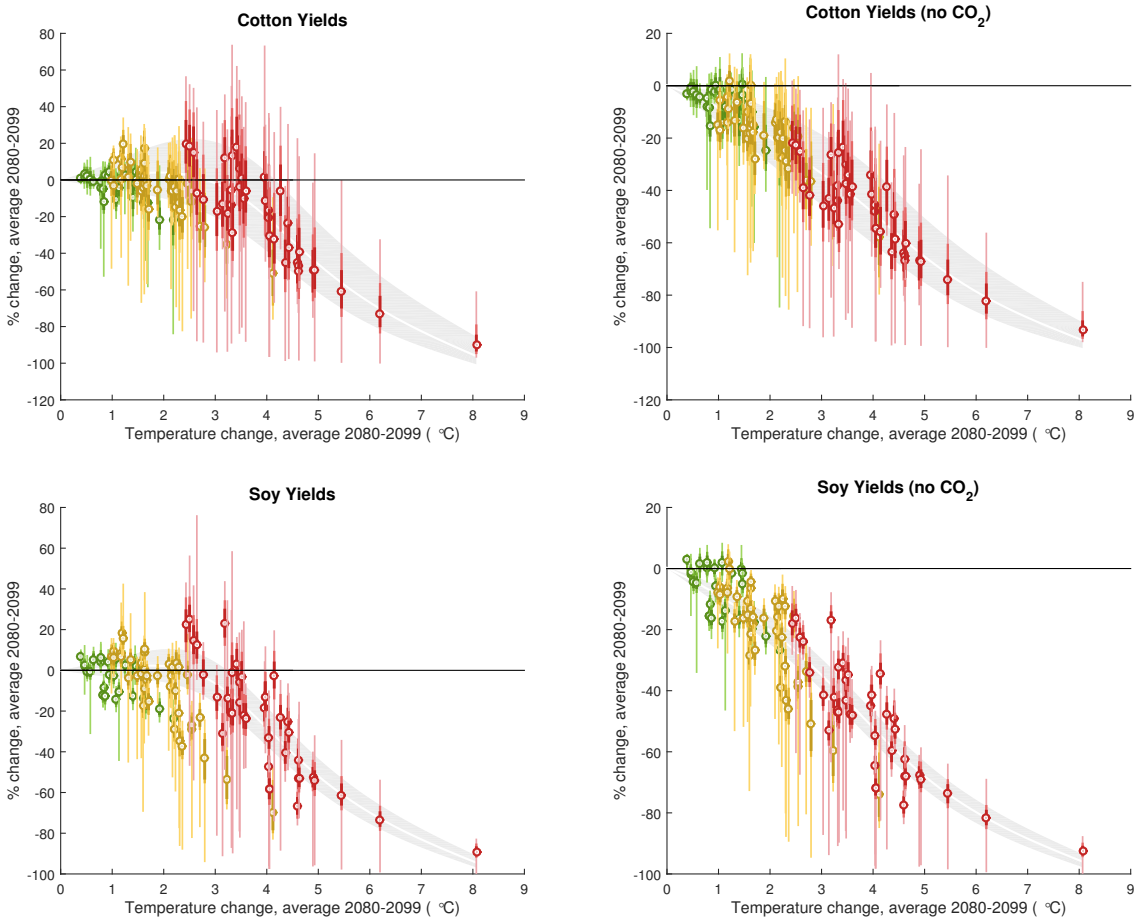

Supplementary Figure S12: **Agriculture damage functions by crop category.** Same as Figures 3A-B, but for cotton and soy only. Approximations to these response surfaces using polynomials, along with statistical uncertainty, are in Table S11. In the left column, discontinuous changes in average impacts and variances in impact between RCP scenarios are driven by the effects of CO2 fertilization.

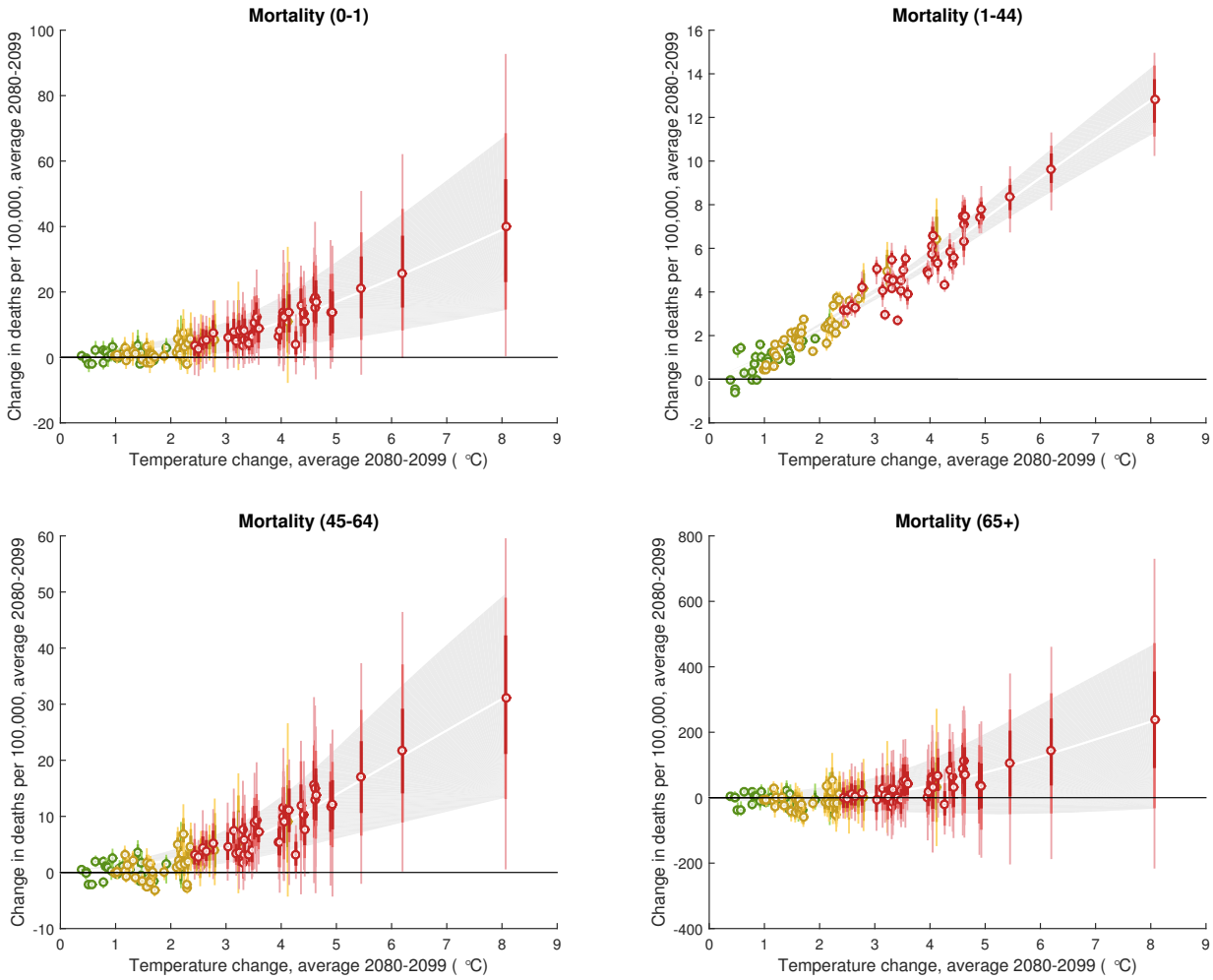

Supplementary Figure S13: **Mortality damage functions by age group.** Same as Figure 3C, but for subgroups by age. Approximations to these response surfaces using polynomials, along with statistical uncertainty, are in Table S12.

Supplementary Table S10: Maize, Wheat and Total Grain Yields in units of percent change, estimated using equation 1

	Maize yields (no CO2 fertilization)				Maize yields			
	linear	2nd	3rd	4th	linear	2nd	3rd	4th
$\Delta GMST$	-14.97***	-22.44***	-13.25***	0.805	-14.49***	-19.21***	-8.139*	-0.465
	(1.113)	(1.625)	(3.797)	(7.642)	(0.920)	(1.997)	(4.486)	(8.679)
$\Delta GMST^2$		1.104***	-1.766	-9.328**		0.697**	-2.758**	-6.888
		(0.211)	(1.070)	(3.938)		(0.271)	(1.258)	(4.523)
$\Delta GMST^3$			0.240***	1.729**			0.289***	1.102
			(0.083)	(0.744)			(0.097)	(0.860)
$\Delta GMST^4$				-0.0939**				-0.0513
				(0.045)				(0.053)
Constant	1.771	11.04***	3.796	-3.766	4.591**	10.44***	1.723	-2.406
	(2.550)	(2.293)	(3.305)	(4.467)	(2.202)	(2.603)	(3.771)	(5.003)
Obs.	26817	26817	26817	26817	26817	26817	26817	26817
Adj. R^2	0.829	0.852	0.857	0.859	0.782	0.791	0.798	0.799
	Wheat yields (no CO2 fertilization)				Wheat yields			
	linear	2nd	3rd	4th	linear	2nd	3rd	4th
$\Delta GMST$	-3.609***	-4.785***	-2.729***	0.783	4.575***	13.59***	9.310*	-18.33**
	(0.194)	(0.352)	(0.859)	(2.068)	(1.131)	(1.771)	(5.146)	(8.954)
$\Delta GMST^2$		0.174***	-0.468**	-2.358**		-1.334***	0.00313	14.88***
		(0.046)	(0.231)	(1.010)		(0.220)	(1.507)	(4.694)
$\Delta GMST^3$			0.0537***	0.426**			-0.112	-3.041***
			(0.018)	(0.188)			(0.119)	(0.893)
$\Delta GMST^4$				-0.0235**				0.185***
				(0.012)				(0.055)
Constant	0.345	1.805***	0.185	-1.705	2.463	-8.730***	-5.356	9.514*
	(0.473)	(0.559)	(0.868)	(1.364)	(2.553)	(2.066)	(3.875)	(4.896)
Obs.	26817	26817	26817	26817	26817	26817	26817	26817
Adj. R^2	0.583	0.591	0.594	0.595	0.215	0.311	0.314	0.339
	Total grain yields (no CO2 fertilization)				Total grain yields			
	linear	2nd	3rd	4th	linear	2nd	3rd	4th
$\Delta GMST$	-10.46***	-15.43***	-9.124***	0.978	-6.975***	-6.317***	-1.403	-7.182
	(0.742)	(1.092)	(2.551)	(5.232)	(0.421)	(1.710)	(4.267)	(7.838)
$\Delta GMST^2$		0.734***	-1.234*	-6.671**		-0.0973	-1.632	1.479
		(0.142)	(0.715)	(2.673)		(0.223)	(1.202)	(4.112)
$\Delta GMST^3$			0.165***	1.235**			0.128	-0.484
			(0.056)	(0.504)			(0.093)	(0.785)
$\Delta GMST^4$				-0.0675**				0.0386
				(0.031)				(0.048)
Constant	1.127	7.286***	2.32	-3.116	3.630***	2.814	-1.059	2.051
	(1.704)	(1.567)	(2.269)	(3.127)	(1.220)	(2.061)	(3.426)	(4.453)
Obs.	26817	26817	26817	26817	26817	26817	26817	26817
Adj. R^2	0.842	0.864	0.868	0.871	0.535	0.535	0.539	0.541

Columns in each cell represent different polynomial regression models. Standard errors are clustered at the level of the climate realization m in parentheses. Stars denote statistical significance: * (p<0.10), ** (p<0.05), *** (p<0.01)

Supplementary Table S11: Cotton, Soy, and Total Yields in units of percent change, estimated using equation 1

	Cotton yields (no CO2 fertilization)				Cotton Yields			
	linear	2nd	3rd	4th	linear	2nd	3rd	4th
$\Delta GMST$	-13.78***	-14.76***	-2.422	-3.663	-11.12***	-0.172	15.99***	-16.87
	(0.575)	(1.620)	(2.368)	(5.428)	(1.074)	(2.957)	(5.631)	(11.070)
$\Delta GMST^2$		0.145	-3.707***	-3.039		-1.619***	-6.667***	11.02*
		(0.259)	(0.674)	(2.957)		(0.474)	(1.651)	(6.078)
$\Delta GMST^3$			0.322***	0.191			0.422***	-3.061**
			(0.053)	(0.571)			(0.131)	(1.193)
$\Delta GMST^4$				0.00829				0.220***
				(0.035)				(0.075)
Constant	7.422***	8.642***	-1.081	-0.413	16.72***	3.134	-9.606**	8.077
	(1.404)	(2.031)	(2.068)	(2.851)	(2.487)	(3.217)	(4.351)	(5.700)
Obs.	26817	26817	26817	26817	26817	26817	26817	26817
Adj. R^2	0.829	0.829	0.84	0.84	0.516	0.573	0.59	0.605
	Soy yields (no CO2 fertilization)				Soy yields			
	linear	2nd	3rd	4th	linear	2nd	3rd	4th
$\Delta GMST$	-14.61***	-18.97***	-7.682*	1.349	-12.60***	-7.040**	9.224	-5.611
	(0.872)	(1.862)	(4.064)	(8.108)	(0.793)	(3.243)	(7.191)	(13.300)
$\Delta GMST^2$		0.645**	-2.879**	-7.739*		-0.822*	-5.900***	2.084
		(0.254)	(1.175)	(4.230)		(0.467)	(2.059)	(7.123)
$\Delta GMST^3$			0.295***	1.252			0.425***	-1.148
			(0.093)	(0.799)			(0.160)	(1.377)
$\Delta GMST^4$				-0.0603				0.0991
				(0.049)				(0.085)
Constant	6.996***	12.41***	3.516	-1.343	15.98***	9.087**	-3.731	4.252
	(2.035)	(2.381)	(3.319)	(4.587)	(2.098)	(3.622)	(5.556)	(7.213)
Obs.	26817	26817	26817	26817	26817	26817	26817	26817
Adj. R^2	0.826	0.835	0.842	0.843	0.573	0.585	0.601	0.603
	Total crop yields (no CO2 fertilization)				Total crop yields			
	linear	2nd	3rd	4th	linear	2nd	3rd	4th
$\Delta GMST$	-12.11***	-16.22***	-7.530**	1.118	-9.128***	-5.338**	4.566	-7.369
	(0.733)	(1.369)	(2.912)	(5.970)	(0.580)	(2.329)	(5.350)	(9.851)
$\Delta GMST^2$		0.607***	-2.105**	-6.760**		-0.561*	-3.653**	2.77
		(0.188)	(0.830)	(3.113)		(0.327)	(1.522)	(5.263)
$\Delta GMST^3$			0.227***	1.143*			0.259**	-1.006
			(0.065)	(0.589)			(0.118)	(1.015)
$\Delta GMST^4$				-0.0578				0.0797
				(0.036)				(0.063)
Constant	4.101**	9.198***	2.351	-2.302	9.570***	4.865*	-2.94	3.481
	(1.695)	(1.819)	(2.465)	(3.416)	(1.563)	(2.648)	(4.175)	(5.388)
Obs.	26817	26817	26817	26817	26817	26817	26817	26817
Adj. R^2	0.859	0.871	0.878	0.879	0.572	0.583	0.594	0.597

Columns in each cell represent different polynomial regression models. Standard errors are clustered at the level of the climate realization m in parentheses. Stars denote statistical significance: * (p<0.10), ** (p<0.05), *** (p<0.01)

Supplementary Table S12: Mortality by age group and all age in units of deaths per $100\,000$, estimated using equation 1

	Infant mortality				Age 1-44 mortality			
	linear	2nd	3rd	4th	linear	2nd	3rd	4th
$\Delta GMST$	4.530***	0.6	-1.972**	-1.822	1.646***	1.446***	1.228***	1.469**
	(0.417)	(0.409)	(0.902)	(2.005)	(0.0359)	(0.114)	(0.295)	(0.710)
$\Delta GMST^2$		0.581***	1.384***	1.304		0.0295**	0.0978	-0.0323
		(0.0592)	(0.278)	(0.975)		(0.0136)	(0.0828)	(0.341)
$\Delta GMST^3$			-0.0671***	-0.0512			-0.00571	0.0199
			(0.0227)	(0.176)			(0.00650)	(0.0618)
$\Delta GMST^4$				-0.001				-0.00161
				(0.0104)				(0.00366)
Constant	-5.894***	-1.014*	1.012	0.931	-0.869***	-0.622***	-0.449	-0.579
	(0.948)	(0.546)	(0.771)	(1.236)	(0.094)	(0.166)	(0.285)	(0.474)
Obs.	26817	26817	26817	26817	26817	26817	26817	26817
Adj. R^2	0.658	0.715	0.718	0.718	0.941	0.942	0.942	0.942
	Age 45-64 mortality				Age 65+ mortality			
	linear	2nd	3rd	4th	linear	2nd	3rd	4th
$\Delta GMST$	3.688***	0.507	-2.572***	-1.567	24.40***	-12.52***	-38.65***	-39.13*
	(1.905)	(3.927)	(4.165)	(10.22)	(3.927)	(4.165)	(10.220)	(22.950)
$\Delta GMST^2$		0.470***	1.432***	0.891		5.460***	13.62***	13.88
		(0.0693)	(0.2550)	(0.9290)		(0.6010)	(3.0940)	(10.9000)
$\Delta GMST^3$			-0.0804***	0.0261			-0.682***	-0.733
			(0.021)	(0.167)			(0.249)	(1.951)
$\Delta GMST^4$				-0.00671				0.00321
				(0.010)				(0.116)
Constant	-5.087***	-1.139**	1.287*	0.747	-49.81***	-3.982	16.61*	16.87
	(0.746)	(0.557)	(0.724)	(1.154)	(9.064)	(5.890)	(8.922)	(14.560)
Obs.	26817	26817	26817	26817	26817	26817	26817	26817
Adj. R^2	0.687	0.746	0.753	0.754	0.353	0.446	0.453	0.453
	All age mortality							
	linear	2nd	3rd	4th				
$\Delta GMST$	5.351***	0.67	-3.233**	-1.623				
	(0.485)	(0.626)	(1.403)	(3.182)				
$\Delta GMST^2$		0.692***	1.911***	1.045				
		(0.094)	(0.418)	(1.547)				
$\Delta GMST^3$			-0.102***	0.0688				
			(0.034)	(0.280)				
$\Delta GMST^4$				-0.0108				
				(0.017)				
Constant	-7.372***	-1.560*	1.516	0.65				
	(1.135)	(0.846)	(1.208)	(1.932)				
Obs.	26817	26817	26817	26817				
Adj. R^2	0.614	0.668	0.673	0.673				

Columns in each cell represent different polynomial regression models. Standard errors are clustered at the level of the climate realization m in parentheses. Stars denote statistical significance: * (p<0.10), ** (p<0.05), *** (p<0.01)

Supplementary Table S13: Energy Expenditures, estimated using equation 1

	Energy expenditures in units of percent change			
	linear	2nd	3rd	4th
$\Delta GMST$	5.314***	2.540***	0.928	-0.878
	(0.138)	(0.325)	(0.847)	(1.887)
$\Delta GMST^2$		0.412***	0.923***	1.919**
		(0.046)	(0.252)	(0.963)
$\Delta GMST^3$			-0.0431**	-0.242
			(0.021)	(0.187)
$\Delta GMST^4$				0.0126
				(0.012)
Constant	-4.466***	-1.061**	0.18	1.111
	(0.409)	(0.490)	(0.773)	(1.163)
Obs.	116	116	116	116
Adj. R^2	0.928	0.958	0.959	0.959

Columns represent different polynomial regression models. Standard errors are clustered at the level of the climate realization m in parentheses. Stars denote statistical significance: * (p<0.10), ** (p<0.05), *** (p<0.01)

Supplementary Table S14: Labor productivity in units of percent change, estimated using equation 1

	Labor supply in low-risk sectors				Labor supply in high-risk sectors			
	linear	2nd	3rd	4th	linear	2nd	3rd	4th
$\Delta GMST$	-0.109***	-0.0650***	-0.0189	-0.0592	-0.527***	-0.422***	-0.275***	-0.317
	(0.005)	(0.009)	(0.018)	(0.043)	(0.015)	(0.043)	(0.103)	(0.253)
$\Delta GMST^2$		-0.00658***	-0.0210***	0.00073		-0.0154***	-0.0615**	-0.0389
		(0.001)	(0.005)	(0.022)		(0.005)	(0.030)	(0.124)
$\Delta GMST^3$			0.00120***	-0.0031			0.00385	-0.00059
			(0.000)	(0.004)			(0.002)	(0.022)
$\Delta GMST^4$				0.00027				0.00028
				(0.000)				(0.001)
Cons.	0.0996***	0.0443***	0.00805	0.0297	0.345***	0.215***	0.0989	0.121
	(0.011)	(0.011)	(0.016)	(0.027)	(0.037)	(0.060)	(0.096)	(0.163)
Obs.	26817	26817	26817	26817	26817	26817	26817	26817
Adj. R^2	0.508	0.518	0.519	0.519	0.847	0.851	0.852	0.852

Columns represent different polynomial regression models. Standard errors are clustered at the level of the climate realization m in parentheses. Stars denote statistical significance: * (p<0.10), ** (p<0.05), *** (p<0.01)

Supplementary Table S15: Crime in units of percent change, estimated using equation 1

	Violent crime				Property crime			
	linear	2nd	3rd	4th	linear	2nd	3rd	4th
$\Delta GMST$	0.884***	1.074***	1.177***	1.338*	0.157***	0.332***	0.466***	0.448
	(0.036)	(0.104)	(0.304)	(0.718)	(0.021)	(0.045)	(0.135)	(0.321)
$\Delta GMST^2$		-0.0291**	-0.0621	-0.151		-0.0267***	-0.0695*	-0.0597
		(0.012)	(0.084)	(0.333)		(0.006)	(0.037)	(0.148)
$\Delta GMST^3$			0.00281	0.0206			0.00364	0.00168
			(0.006)	(0.059)			(0.003)	(0.026)
$\Delta GMST^4$				-0.00114				0.000125
				(0.004)				(0.002)
Constant	-0.161	-0.384**	-0.462	-0.545	0.142**	-0.0623	-0.163	-0.154
	(0.103)	(0.168)	(0.301)	(0.494)	(0.058)	(0.075)	(0.132)	(0.216)
Obs.	14757	14757	14757	14757	14757	14757	14757	14757
Adj. R^2	0.858	0.863	0.863	0.863	0.434	0.498	0.503	0.503

Columns represent different polynomial regression models. Standard errors are clustered at the level of the climate realization m in parentheses. Stars denote statistical significance: * (p<0.10), ** (p<0.05), *** (p<0.01)

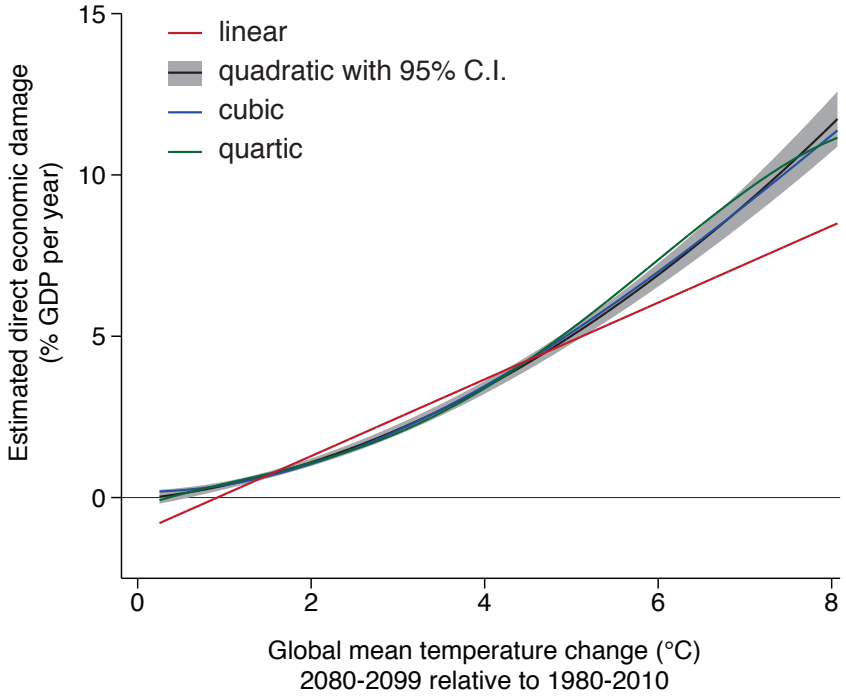

Supplementary Figure S14: **Estimating different functional forms for expected total direct damage.** Alternative polynomial specifications for conditional mean in Figure 5A (coefficients are reported in Table S16). Third and fourth order polynomials lie with the confidence interval for the quadratic model, which is selected as the benchmark model.

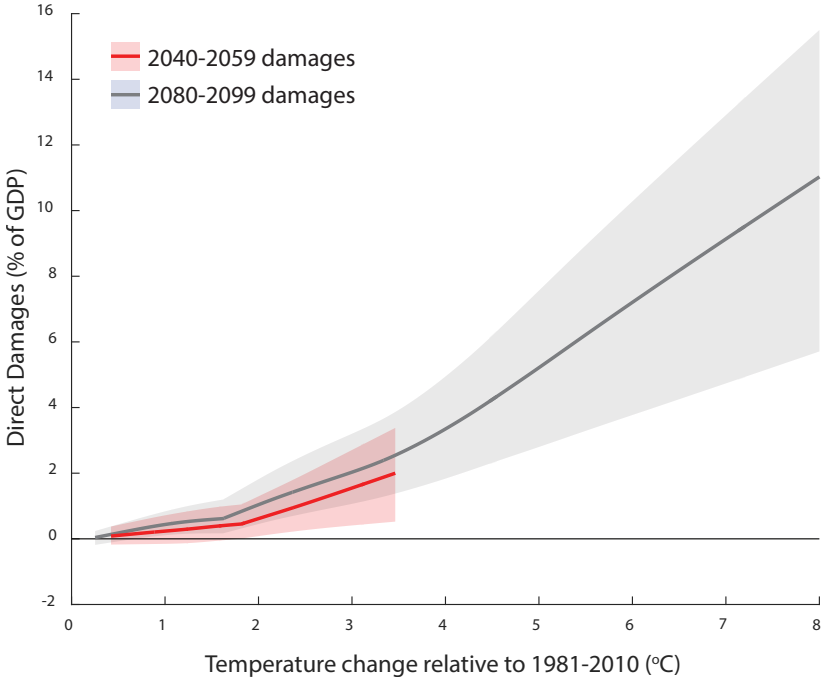

Supplementary Figure S15: **Comparison of aggregate damage function using mid-century outcomes.** Comparing the aggregate national damage function shown in Figure 5A (black) with an analogous damage function computed using projections from 2040-2059 (red).

Supplementary Table S16: Regressions of total direct damage on global mean temperature change

Polynomial	Total Direct Damages			
order:	linear	2nd	3rd	4th
$\Delta GMST$	1.189***	0.283**	-0.0325	0.907*
	(0.082)	(0.110)	(0.233)	(0.469)
$\Delta GMST^2$		0.146***	0.249***	-0.281
		(0.017)	(0.074)	(0.251)
$\Delta GMST^3$			-0.00901	0.0989**
			(0.006)	(0.048)
$\Delta GMST^4$				-0.00697**
				(0.003)
Constant	-1.091***	-0.0547	0.182	-0.292
	(0.179)	(0.134)	(0.185)	(0.248)
Obs.	109000	109000	109000	109000
Adj. R^2	0.726	0.774	0.775	0.777

Standard errors are clustered at the level of the climate realization m in parentheses. Stars denote statistical significance: * (p<0.10), ** (p<0.05), *** (p<0.01)

Supplementary Table S17: Bounds of 90% credible interval for probability mass in aggregate damage function shown in Figure 5A

$\Delta GMST$	5th percentile	95th percentile
1	-0.32	1.14
1.5	-0.14	1.69
2	0.09	2.31
3	0.67	3.79
4	1.45	5.57
5	2.41	7.65
6	3.56	10.04
7	4.90	12.74
8	6.42	15.74

Units are percentage of GDP.

K Valuing risk and inequality for total direct damages

Disutility from risk and inequality for individuals are well understood, but appropriate values describing risk aversion and inequality aversion at a national-level remains an area of active research, so we simply demonstrate how one might adjust the damage function in Figure 5A using a range of plausible values (2-8 for both parameters) (*89, 45*). To construct *inequality-neutral, certainty-equivalent damage functions*—the economic losses equal in value to projected probabilistic impacts but suffered uniformly across the country with certainty—we first compute the cost of economic risks for each county (including the cost of uncertainty) and then the nationally aggregated cost of these risks adjusted for their unequal distribution.

Overall, we find that inequality of impacts across locations in the US tends to increase the value of climate damages more than risk, although both effects can be substantial and interact (Figure S16). Accounting for inequality tends to increase the social valuation of damages by a factor of $\sim$1.4-3.1 for moderate changes in global mean temperature (3°C) and $\sim 1.3 - 4.6$ for large changes (8°C), depending on assumed values for inequality aversion. Accounting for risk aversion increases damages by a factor of ~ 1.1 in most cases for low levels of inequality aversion but can lead to a doubling of costs for high warming and high inequality aversion (Figure S16 and Table S18). Losses valued at 20% of GDP occur at GMST warming of 5-6°C for moderate values of risk and inequality aversion.

Example calculation of inequality-neutral, certainty-equivalent damages

Following (*41*) (which only accounted for risk and uncertainty in two sectors), we calculate the risk- and inequality-premiums on total climate change damages by assuming that each county is composed of homogenous agents with an income equal to that county's per capita income. While still an imperfect approximation, it respects regional variations in incomes far more than approaches that assume uniform incomes across the entire country or world. County-level incomes and populations were taken from the BEA (*90*). For each county j, we calculate the certainty-equivalent income per capita c^*, where

$$u(c_j^*) = \sum_i p_i u(c_{ij}). \tag{2}$$

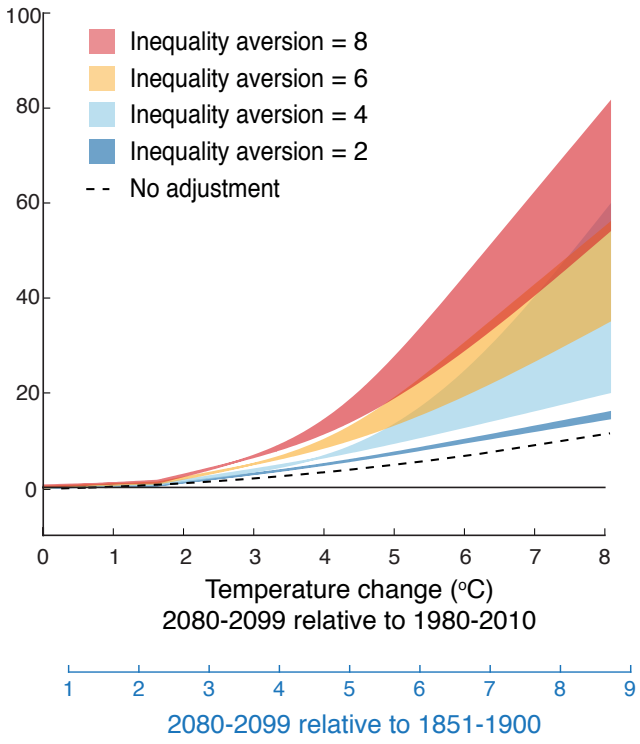

Supplementary Figure S16: **Example valuation of risk and inequality in aggregate damages. (A)** National inequality-neutral certainty-equivalent loss equal in value to direct damages under different assumptions regarding coefficients of inequality aversion and risk aversion. Shaded regions span results for risk aversion values between 2 and 8 (lower and upper bounds). Values tabulated in Table S18. Dashed line is same as curve in Figure 5A.

In this expression, the indices i denote states of the world and p_i their associated probabilities. We employ an isoelastic utility function with relative risk aversion RRA,

$$u(c) = \frac{c^{1-\mathrm{RRA}}}{1-\mathrm{RRA}} \tag{3}$$

which implies that

$$c_j^* = \Big(\sum_i p_i c_{ij}^{1-\mathrm{RRA}}\Big)^{1/(1-\mathrm{RRA})}. \tag{4}$$

Note that, when $\mathrm{RRA} = 0$, c_j^* is simply the expected income of j.

We then calculate the inequality-neutral certainty-equivalent income loss. To do this, we find the equal-percentage loss that, if forfeited by all agents with certainty, yields the same welfare as the actual cross-sectional distribution of certainty equivalent losses c_j^*. Denoting the inequality-neutral certainty-

Supplementary Table S18: Adjusting damages for inequality and risk

		IA = 2		IA = 4		IA = 6		IA = 8	
	CRRA:	2	8	2	8	2	8	2	8
ΔT	Avg. damage (% GDP)	Inequality-neutral certainty-equivalent damage (% GDP)							
1 °C	0.47	0.56	0.58	0.74	0.74	0.97	0.93	1.25	1.17
2 °C	1.23	1.41	1.45	1.89	1.69	2.45	2.22	3.11	2.78
3 °C	2.27	3.22	3.31	4.23	3.76	5.39	5.46	6.93	7.23
4 °C	3.61	5.22	5.40	6.86	7.15	8.98	10.68	12.08	14.99
5 °C	5.24	7.55	7.90	10.01	13.95	13.97	19.70	19.91	28.58
6 °C	7.17	10.04	10.66	13.47	25.49	20.36	31.63	30.24	46.06
7 °C	9.38	12.58	13.53	17.08	41.52	27.85	44.02	42.27	64.11
8 °C	11.88	15.13	16.45	20.74	60.13	35.93	54.54	55.17	79.92

CRRA = Constant relative risk aversion. IA = Inequality aversion. ΔT = global mean temperature change from 1980-2010 baseline.

equivalent income loss as ψ and county populations as N_j, we compute welfare:

$$\sum_j N_j v(c_j^*) = \sum_j N_j v(c_j^0(1-\psi)), \tag{5}$$

where c_j^0 is the per capita income of county j in the absence of climate impacts and the welfare function

$$v(c) = \frac{c^{1-\mathrm{IA}}}{1-\mathrm{IA}} \tag{6}$$

implies that society has a coefficient of inequality aversion IA among contemporaries.

Note that when $\mathrm{IA} = 0$, this reduces to

$$\sum_j N_j c_j^* = (1-\psi)\sum_j N_j c_j^0 \tag{7}$$

$$\psi = \sum_j N_j (c_j^0 - c_j^*) / \sum_j N_j c_j^0 \tag{8}$$

so ψ is simply the ratio of total certainty-equivalent damages as a fraction of total income in the absence of climate impacts. For a given value of RRA, the "inequality premium" can be defined as the difference between ψ computed at a selected value of IA and the same variables computed at $\mathrm{IA} = 0$. Similarly, for a given value of IA, the "risk premium" can be defined as the difference between ψ computed at a selected value of RRA and the same variables computed at $\mathrm{RRA} = 0$

Table S18 tabulates the inequality-neutral certainty-equivalent income loss for the the US under ranges of IA and RRA at integer values of ΔGMST. These values are plotted in Figure S16.

Note also that we have intentionally chosen to compute the premium among contemporaries for unequal risk, rather than a risk premium for inequality among contemporaries. We have chosen to focus on the former because we think it more accurately captures how society understands and practically values the impacts of climate change. Relying on the latter implies that decision-makers imagine each potential future realization of the national income distribution, weigh their aversion to each scenario independently, and then assign probabilities to each of these potential realizations. While feasible, we think latter approach is less intuitive as well as less desirable, as it ignores the private risk borne by individuals and only considers risk related to the taste for socio-economic structure in future populations.

L Evaluation and comparison of CGE model results

In response to the direct damages due to climate change, it is possible that the US economy will reallocate resources in order to cope with these changes. To provide a sense for how such reallocation might moderate these direct damages, we develop a computable general equilibrium (CGE) model that reallocates capital across locations and industries in response to the capital and productivity losses described above during each period of a century-long integration. Theoretically, it is possible for these reallocations to reduce damages, as production migrates away from adverse climates, or for them to increase damages, as losses in one location alter economic decisions in other locations and/or later periods by influencing markets via prices. When using this approach, we cannot account for non-market valuations, so loss of life is valued only using foregone earnings while crime and inequality are not accounted for.

We find that the most important insight from accounting for these dynamics is that direct damages alter capital investment decisions by altering the prices of capital and different outputs—an effect that

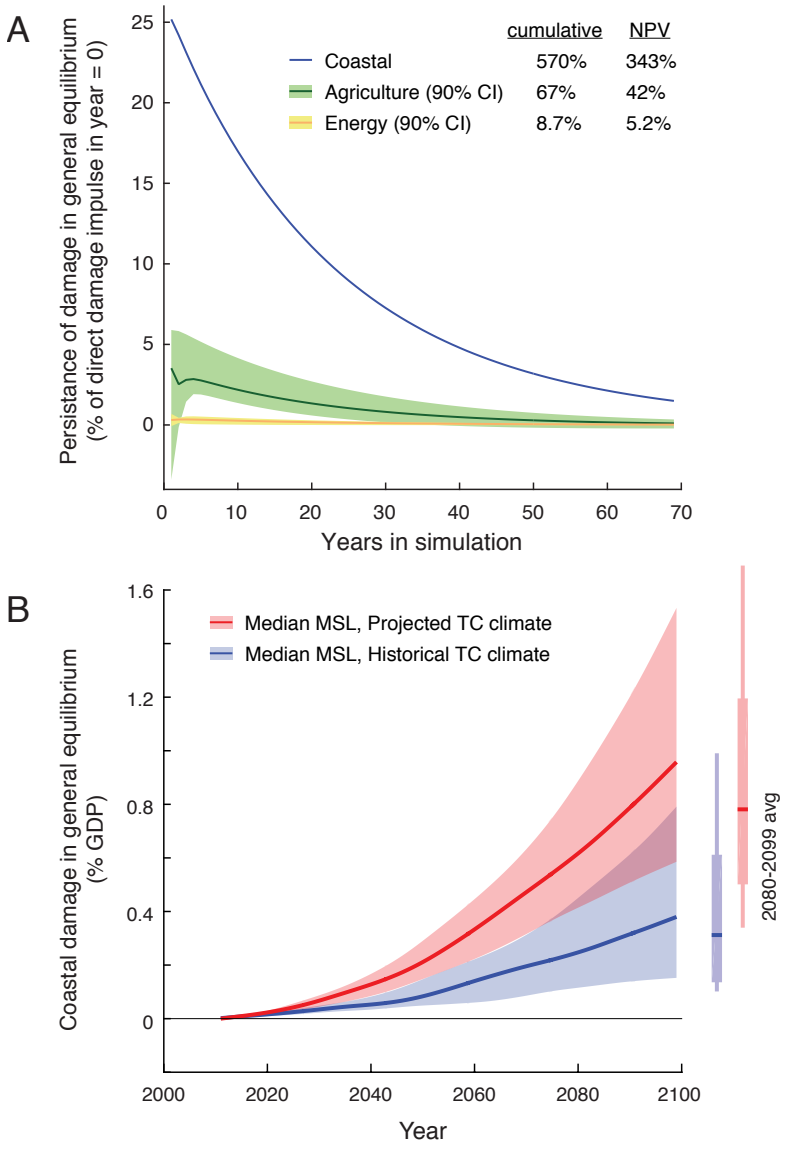

Supplementary Figure S17: **Example CGE dynamics in response to direct climate damages. (A)** Each sector within the CGE model is separately damaged for a single year using the empirically calculated damages from 2030 for that sector. Damages used are from RCP 8.5 for each of the 44 climate realizations. The effect on GDP due to reallocation in response to this single year shock is tracked throughout the model lifetime. Lagged losses to the aggregate economy resulting from direct impacts in three sectors are shown. Values are % of damage in the year of the shock. CI denote ranges from multiple climate realizations. Cumulative effects are integrals of response out to $\sim \infty$, not including loss in year 0. Net present values (NPV) are cumulative losses discounted at 3% yr^{-1}, reflecting the central discount rate adopted by ref. (*8*). **(B)** Projected coastal damage in general equilibrium (compare to Figure 4G). We perform a Monte Carlo simulation of coastal damages from historical and projected hurricanes. Projected hurricane activity under climate change is described in Section H. Results use 100 draws and tracks direct and indirect damages due to hurricanes within the CGE model.

differs based on how climate affects each sector. In an experiment where different sectors are shocked by direct losses for only a single year and the economy is allowed to adjust (Figure S17A), we see large persistent GDP losses due to cyclones, cumulatively equal to 570% of the initial shock, because cyclone-induced depreciation elevates national demand for capital, raising its price and lowering capital-to-labor ratios in subsequent years. This result is broadly consistent with empirical findings that direct capital losses underestimate economic losses to cyclones by roughly a factor of ten (*53, 91*)). Accounting for this effect substantially increases the projected cost of coastal impacts, roughly doubling end-of-century losses to 1% of GDP when accounting for projected changes in cyclones (Figure S17B). Impacts on agriculture have similar effects by altering investment decisions, via prices, in downstream manufacturing industries where agricultural products are inputs, whereas energy impacts do not (Figure S17A).

To examine whether reallocation decisions over the next century increases or decreases costs on net, we simulate the trajectory of the future economy under each climate realization, imposing our computed direct damages each period. When direct damages are imposed on only one sector at a time, the total end-of-century economic loss may be larger or smaller than the corresponding direct damages estimate, depending on the sector and climate realization (Figure 5D). Costs of mortality are dramatically lower because of how they are valued: foregone earnings in the market equilibrium are much smaller than the non-market VSL used to compute direct damages.

However, in a complete simulation where national markets are simultaneously forced by direct damages in all sectors, net market losses in general equilibrium are larger than direct damages by $\sim$50% (mortality is excluded from both; only one out of 39 projections is slightly lower at 98.3% of direct damages). These simulations are relatively coarse approximations of a complex national economy, but they are the first to account for spatiotemporal and cross-sector correlations of climate damages in general equilibrium using highly resolved climate projections and empirical impact estimates.

The full description of the RHG-MUSE model can be found in (*41*).

Figure 5D: Comparison of CGE damages to direct damages by sector We compare CGE adjusted losses with direct damage losses by separately calculating damages within the CGE from each sector, and again for all sectors simultaneously. All impacts use the median values for each impact function, using one weather draw for each model (due to computational costs). Each model run used to construct Figure

5D is shown in Figure S18 (same values) displayed against the GMST response in the corresponding climate realization. Nonparametric regression lines with bootstrapped confidence intervals are shown. In general, there is no clear pattern in the ratio of CGE to direct damages in relation to the magnitude of the GMST change.

The *All* category in Figures 5D and S18 shows the ratio of all damages (less mortality) in the CGE to all direct damages (less mortality). Mortality is removed from both the numerator and denominator in this comparison for consistency because CGE mortality is valued based only on foregone earnings, whereas direct damages of mortality is valued using a VSL, which contains both foregone earnings as well as non-market valuations of life. The ratio of these mortality costs are shown in Figures 5D and S18 for completeness, but omitted in the *All* category for clarity and consistency. We check that this exclusion does not distort this comparison in a systematic way in Figure S19, where we compare the ratio of all CGE to all direct costs for each model when mortality is and is not included in the CGE total (it is not included in directs costs for either case). As expected, excluding CGE mortality costs lowers the ratio by roughly a constant percentage that does not vary systematically with the ratio of the remaining costs.

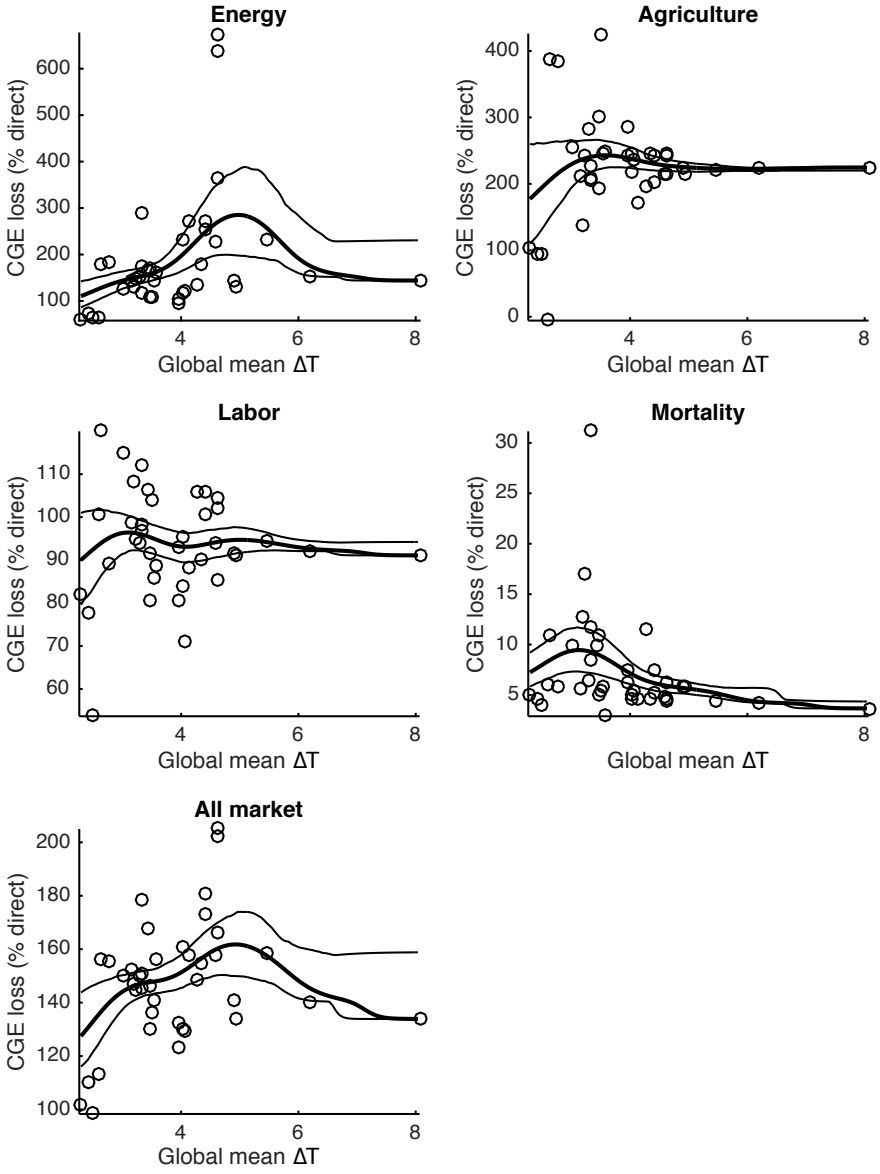

Supplementary Figure S18: **CGE costs relative to direct damages in the same sector as a function of GMST change.** Data are same values as plotted in Figures 5D, except shown as a function of GMST changes. Regressions are non-parametric regressions with bootstrap 95% confidence intervals.

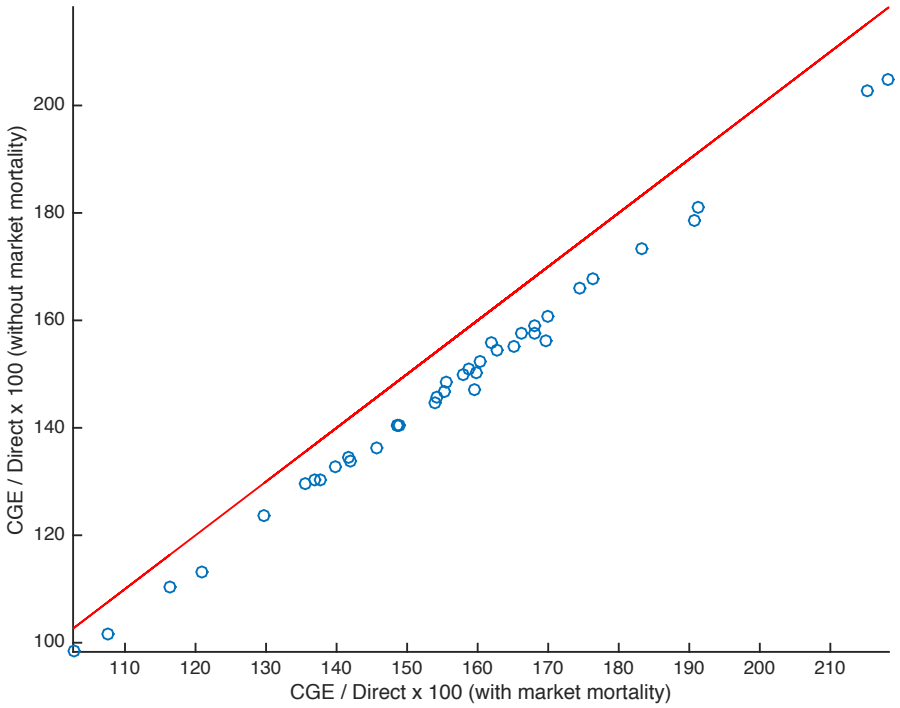

Supplementary Figure S19: **Comparing the ratio of *All* CGE costs to direct costs when mortality is and is not included in CGE costs.** VSL valuations of mortality are not included in direct costs for either case. Blue circles are model outcomes for each climate realization. Red line is the the line $y = x$.

References

1. W. D. Nordhaus, Optimal greenhouse-gas reductions and tax policy in the "dice" model**.** *Am. Econ. Rev.* **83**, 313–317 (1993).

2. M. L. Weitzman, On modeling and interpreting the economics of catastrophic climate change. *Rev. Econ. Stat.* **91**, 1–19 (2009). doi:10.1162/rest.91.1.1

3. K. C. de Bruin, R. B. Dellink, R. S. Tol, AD-DICE: An implementation of adaptation in the DICE model. *Clim. Change* **95**, 63–81 (2009). doi:10.1007/s10584-008-9535-5

4. A. Costinot, D. Donaldson, C. Smith, Evolving comparative advantage and the impact of climate change in agricultural markets: Evidence from 1.7 million fields around the world. *J. Polit. Econ.* **124**, 205–248 (2016). doi:10.1086/684719

5. D. Lemoine, C. Traeger, Watch your step: Optimal policy in a tipping climate. *Am. Econ. J. Econ. Policy* **6**, 137–166 (2014). doi:10.1257/pol.6.1.137

6. Y. Cai, K. L. Judd, T. M. Lenton, T. S. Lontzek, D. Narita, Environmental tipping points significantly affect the cost-benefit assessment of climate policies. *Proc. Natl. Acad. Sci. U.S.A.* **112**, 4606–4611 (2015). doi:10.1073/pnas.1503890112 Medline

7. N. Stern, *Stern Review: The Economics of Climate Change* (Cambridge Univ. Press, 2006).

8. Interagency Working Group on Social Cost of Carbon, Technical support document: Social cost of carbon for regulatory impact analysis under Executive Order 12866, *Tech. rep.*, United States Government (2010).

9. R. L. Revesz, P. H. Howard, K. Arrow, L. H. Goulder, R. E. Kopp, M. A. Livermore, M. Oppenheimer, T. Sterner, Global warming: Improve economic models of climate change. *Nature* **508**, 173–175 (2014). doi:10.1038/508173a Medline

10. N. Stern, The structure of economic modeling of the potential impacts of climate change: Grafting gross underestimation of risk onto already narrow science models. *J. Econ. Lit.* **51**, 838–859 (2013). doi:10.1257/jel.51.3.838

11. R. S. Tol, The economic effects of climate change. *J. Econ. Perspect.* **23**, 29–51 (2009). doi:10.1257/jep.23.2.29

12. R. S. Pindyck, Climate change policy: What do the models tell us? *J. Econ. Lit.* **51**, 860–872 (2013). doi:10.1257/jel.51.3.860

13. S. M. Hsiang, Climate econometrics. *Annu. Rev. Resour. Econ.* **8**, 43–75 (2016). doi:10.1146/annurev-resource-100815-095343

14. T. A. Carleton, S. M. Hsiang, Social and economic impacts of climate. *Science* **353**, aad9837 (2016). doi:10.1126/science.aad9837 Medline

15. R. E. Kopp, S. M. Hsiang, M. Oppenheimer, *Impacts World 2013 Conference Proceedings* (Potsdam Institute for Climate Impact Research, Potsdam, Germany, 2013), pp. 834–843.

16. W. Pizer, M. Adler, J. Aldy, D. Anthoff, M. Cropper, K. Gillingham, M. Greenstone, B. Murray, R. Newell, R. Richels, A. Rowell, S. Waldhoff, J. Wiener, Using and improving the social cost of carbon. *Science* **346**, 1189–1190 (2014). doi:10.1126/science.1259774 Medline

17. M. Burke, M. Craxton, C. D. Kolstad, C. Onda, H. Allcott, E. Baker, L. Barrage, R. Carson, K. Gillingham, J. Graff-Zivin, M. Greenstone, S. Hallegatte, W. M. Hanemann, G. Heal, S. Hsiang, B. Jones, D. L. Kelly, R. Kopp, M. Kotchen, R. Mendelsohn, K. Meng, G. Metcalf, J. Moreno-Cruz, R. Pindyck, S. Rose, I. Rudik, J. Stock, R. S. J. Tol, Opportunities for advances in climate change economics. *Science* **352**, 292–293 (2016). doi:10.1126/science.aad9634 Medline

18. Materials and methods are available online as supplementary materials.

19. D. Rasmussen, M. Meinshausen, R. E. Kopp, Probability-weighted ensembles of U.S. county-level climate projections for climate risk analysis. *J. Appl. Meteorol. Climatol.* **55**, 2301–2322 (2016). doi:10.1175/JAMC-D-15-0302.1

20. D. P. van Vuuren, J. Edmonds, M. Kainuma, K. Riahi, A. Thomson, K. Hibbard, G. C. Hurtt, T. Kram, V. Krey, J.-F. Lamarque, T. Masui, M. Meinshausen, N. Nakicenovic, S. J. Smith, S. K. Rose, The representative concentration pathways: An overview. *Clim. Change* **109**, 5–31 (2011). doi:10.1007/s10584-011-0148-z

21. K. E. Taylor, R. J. Stouffer, G. A. Meehl, An overview of CMIP5 and the experiment design. *Bull. Am. Meteorol. Soc.* **93**, 485–498 (2012). doi:10.1175/BAMS-D-11-00094.1

22. W. Schlenker, M. J. Roberts, Nonlinear temperature effects indicate severe damages to U.S. crop yields under climate change. *Proc. Natl. Acad. Sci. U.S.A.* **106**, 15594–15598 (2009). doi:10.1073/pnas.0906865106 Medline

23. J. M. McGrath, D. B. Lobell, Regional disparities in the CO_2 fertilization effect and implications for crop yields. *Environ. Res. Lett.* **8**, 014054 (2013). doi:10.1088/1748-9326/8/1/014054

24. O. Deschênes, M. Greenstone, Climate change, mortality, and adaptation: Evidence from annual fluctuations in weather in the US. *Am. Econ. J. Appl. Econ.* **3**, 152–185 (2011). doi:10.1257/app.3.4.152

25. A. Barreca, K. Clay, O. Deschênes, M. Greenstone, J. S. Shapiro, Adapting to climate change: The remarkable decline in the US temperature-mortality relationship over the twentieth century. *J. Polit. Econ.* **124**, 105–159 (2016). doi:10.1086/684582

26. B. Jacob, L. Lefgren, E. Moretti, The dynamics of criminal behavior. *J. Hum. Resour.* **42**, 489–527 (2007). doi:10.3368/jhr.XLII.3.489

27. M. Ranson, Crime, weather, and climate change. *J. Environ. Econ. Manage.* **67**, 274–302 (2014). doi:10.1016/j.jeem.2013.11.008

28. J. Graff Zivin, M. Neidell, Temperature and the allocation of time: Implications for climate change. *J. Labor Econ.* **32**, 1–26 (2014). doi:10.1086/671766

29. J. A. Rising, S. M. Hsiang, SSRN Working Paper 2458129 ; available at SSRN: https://ssrn.com/abstract=2458129 (2014).

30. S. M. Hsiang, M. Burke, E. Miguel, Quantifying the influence of climate on human conflict. *Science* **341**, 1235367 (2013). doi:10.1126/science.1235367 Medline

31. U.S. Energy Information Administration, The national energy modeling system: An overview, Tech. Rep. DOE/EIA-0581 (2009); available at http://www.eia.gov/oiaf/aeo/overview/index.html.

32. H. Willoughby, R. Darling, M. Rahn, Parametric representation of the primary hurricane vortex. Part II: A new family of sectionally continuous profiles. *Mon. Weather Rev.* **134**, 1102–1120 (2006). doi:10.1175/MWR3106.1

33. I. Warren, H. Bach, MIKE 21: A modelling system for estuaries, coastal waters and seas. *Environ. Softw.* **7**, 229–240 (1992). doi:10.1016/0266-9838(92)90006-P

34. T. M. Hall, S. Jewson, Statistical modelling of North Atlantic tropical cyclone tracks. *Tellus, Ser. A, Dyn. Meterol. Oceanogr.* **59**, 486–498 (2007). doi:10.1111/j.1600-0870.2007.00240.x

35. K. A. Emanuel, Downscaling CMIP5 climate models shows increased tropical cyclone activity over the 21st century. *Proc. Natl. Acad. Sci. U.S.A.* **110**, 12219–12224 (2013). doi:10.1073/pnas.1301293110 Medline

36. R. E. Kopp, R. M. Horton, C. M. Little, J. X. Mitrovica, M. Oppenheimer, D. J. Rasmussen, B. H. Strauss, C. Tebaldi, Probabilistic 21st and 22nd century sea-level projections at a global network of tide-gauge sites. *Earths Futur.* **2**, 383–406 (2014). doi:10.1002/2014EF000239

37. U.S. Environmental Protection Agency, National Center for Environmental Economics, Valuing mortality risk reductions for environmental policy: A white paper, *Tech. rep.* (2010).

38. P. Heaton, *Hidden in Plain Sight* (RAND Corporation, 2010).

39. C. J. Vörösmarty, P. Green, J. Salisbury, R. B. Lammers, Global water resources: Vulnerability from climate change and population growth. *Science* **289**, 284–288 (2000). Medline

40. S. M. Hsiang, Essays on the social impacts of climate, Ph.D. thesis, Columbia University (2011).

41. T. Houser *et al*., *Economic Risks of Climate Change: An American Prospectus* (Columbia Univ. Press, 2015).

42. M. Burke, S. M. Hsiang, E. Miguel, Global non-linear effect of temperature on economic production. *Nature* **527**, 235–239 (2015). doi:10.1038/nature15725 Medline

43. E. Hawkins, R. Sutton, The potential to narrow uncertainty in regional climate predictions. *Bull. Am. Meteorol. Soc.* **90**, 1095–1107 (2009). doi:10.1175/2009BAMS2607.1

44. W. K. Viscusi, J. E. Aldy, *J. Risk Uncertain.* **27**, 5–76 (2003). doi:10.1023/A:1025598106257

45. C. Gollier, *Pricing the Planet's Future: The Economics of Discounting in an Uncertain World* (Princeton Univ. Press, 2013).

46. M. L. Weitzman, A Review of the *Stern Review on the Economics of Climate Change*. *J. Econ. Lit.* **45**, 703–724 (2007). doi:10.1257/jel.45.3.703

47. J. A. Patz, D. Campbell-Lendrum, T. Holloway, J. A. Foley, Impact of regional climate change on human health. *Nature* **438**, 310–317 (2005). doi:10.1038/nature04188 Medline

48. S. M. Hsiang, Temperatures and cyclones strongly associated with economic production in the Caribbean and Central America. *Proc. Natl. Acad. Sci. U.S.A.* **107**, 15367–15372 (2010). doi:10.1073/pnas.1009510107 Medline

49. G.-R. Walther, E. Post, P. Convey, A. Menzel, C. Parmesan, T. J. C. Beebee, J.-M. Fromentin, O. Hoegh-Guldberg, F. Bairlein, Ecological responses to recent climate change. *Nature* **416**, 389–395 (2002). doi:10.1038/416389a Medline

50. O. Deschênes, M. Greenstone, The economic impacts of climate change: Evidence from agricultural output and random fluctuations in weather. *Am. Econ. Rev.* **97**, 354–385 (2007). doi:10.1257/000282807780323604

51. M. Burke, K. Emerick, Adaptation to climate change: Evidence from US agriculture. *Am. Econ. J. Econ. Policy* **8**, 106–140 (2016). doi:10.1257/pol.20130025

52. T. Deryugina, S. M. Hsiang, NBER Working Paper 20750 (NBER, 2014); http://www.nber.org/papers/w20750.

53. S. M. Hsiang, A. Jina, NBER Working Paper 20352 (NBER, 2014); http://www.nber.org/papers/w20352.

54. T. D. Mitchell, Pattern scaling: An examination of the accuracy of the technique for describing future climates**.** *Clim. Change* **60**, 217–242 (2003). doi:10.1023/A:1026035305597

55. M. Meinshausen, S. C. B. Raper, T. M. L. Wigley, Emulating coupled atmosphere-ocean and carbon cycle models with a simpler model, MAGICC6 – Part 1: Model description and calibration. *Atmos. Chem. Phys.* **11**, 1417–1456 (2011). doi:10.5194/acp-11-1417-2011

56. J. Rogelj, M. Meinshausen, R. Knutti, Global warming under old and new scenarios using IPCC climate sensitivity range estimates. *Nat. Clim. Chang.* **2**, 248–253 (2012). doi:10.1038/nclimate1385

57. M. Collins *et al*., *Climate Change 2013: The Physical Science Basis. Contribution of Working Group I to the Fifth Assessment Report of the Intergovernmental Panel on Climate Change*, T. Stocker *et al.*, Eds. (Cambridge Univ. Press, Cambridge, United Kingdom and New York, NY, USA, 2013), pp. 1029–1136.

58. L. Brekke, A. Wood, T. Pruitt, Downscaled CMIP3 and CMIP5 Climate Projections: Release of Downscaled CMIP5 Climate Projections, Comparison with Preceding Information, and Summary of User Needs, *Tech. Rep.*, USBR Tech Memo., Denver, Colorado (2014).

59. A. Arguez, I. Durre, S. Applequist, R. S. Vose, M. F. Squires, X. Yin, R. R. Heim Jr., T. W. Owen, NOAA's 1981–2010 U.S. climate normals: An overview. *Bull. Am. Meteorol. Soc.* **93**, 1687–1697 (2012). doi:10.1175/BAMS-D-11-00197.1

60. A. W. Wood, L. R. Leung, V. Sridhar, D. P. Lettenmaier, Hydrologic implications of dynamical and statistical approaches to downscaling climate model outputs. *Clim. Change* **62**, 189–216 (2004). doi:10.1023/B:CLIM.0000013685.99609.9e

61. A. Gelman, J. B. Carlin, H. S. Stern, D. B. Rubin, *Bayesian Data Analysis* (Chapman & Hall/CRC, 2004).

62. U.S. Energy Information Administration, *Annual Energy Outlook 2013* (US DOE/EIA, 2013).

63. U.S. Energy Information Administration, State electricity profiles (2014). Available at www.eia.gov/electricity/state/archive/2012/ on 16 June 2014.

64. U.S. Energy Information Administration, Total energy consumption, price, and expenditure estimates (2014). www.eia.gov/state/seds/data.cfm?incfile=/state/seds/sep_fuel/html/fuel_te.html&sid=US.

65. T. R. Knutson, J. J. Sirutis, G. A. Vecchi, S. Garner, M. Zhao, H.-S. Kim, M. Bender, R. E. Tuleya, I. M. Held, G. Villarini, Dynamical downscaling projections of twenty-first-century Atlantic hurricane activity: CMIP3 and CMIP5 model-based scenarios. *J. Clim.* **26**, 6591–6617 (2013). doi:10.1175/JCLI-D-12-00539.1

66. IMPLAN Group, 51 states totals package (2011); https://implan.com

67. F. C. Curriero, K. S. Heiner, J. M. Samet, S. L. Zeger, L. Strug, J. A. Patz, Temperature and mortality in 11 cities of the eastern United States. *Am. J. Epidemiol.* **155**, 80–87 (2002). doi:10.1093/aje/155.1.80 Medline

68. B. G. Anderson, M. L. Bell, Weather-related mortality: How heat, cold, and heat waves affect mortality in the United States. *Epidemiology* **20**, 205–213 (2009). doi:10.1097/EDE.0b013e318190ee08 Medline

69. G. B. Anderson, M. L. Bell, Heat waves in the United States: Mortality risk during heat waves and effect modification by heat wave characteristics in 43 U.S. communities. *Environ. Health Perspect.* **119**, 210–218 (2011). doi:10.1289/ehp.1002313 Medline

70. O. Seppanen, W. Fisk, Q. Lei, *Lawrence Berkeley National Laboratory Technical Report* (2006). https://indoor.lbl.gov/sites/all/files/lbnl-60946.pdf.

71. S. T. Berry, M. J. Roberts, W. Schlenker, *NBER Working Paper 18659* (2012). http://www.nber.org/papers/w18659.

72. S. Hsiang, D. Lobell, M. Roberts, W. Schlenker, *SSRN Working Paper 2977571* (2013). http://ssrn.com/abstract=2977571.

73. A. C. Fisher, W. M. Hanemann, M. J. Roberts, W. Schlenker, The economic impacts of climate change: Evidence from agricultural output and random fluctuations in weather: Comment. *Am. Econ. Rev.* **102**, 3749–3760 (2012). doi:10.1257/aer.102.7.3749

74. W. J. Sacks, D. Deryng, J. A. Foley, N. Ramankutty, Crop planting dates: An analysis of global patterns. *Glob. Ecol. Biogeogr.* **19**, 607–620 (2010). doi:10.1111/j.1466-8238.2010.00551.x

75. Center for Disease Control and Prevention, Compressed Mortality File 1999-2010 on CDC WON- DER Online Database, released January 2013, Data are compiled from Compressed Mortality File 1999-2010 Series 20 No. 2P (2013). Accessed at http://wonder.cdc.gov/cmf-icd10.html on 22 March 2014.

76. M. J. Roberts, W. Schlenker, Identifying supply and demand elasticities of agricultural commodities: Implications for the US ethanol mandate. *Am. Econ. Rev.* **103**, 2265–2295 (2013). doi:10.1257/aer.103.6.2265

77. Bureau of Labor Statistics, Occupational employment statistics, http://data.bls.gov/oes/ (2014). Accessed on 20 March 2014.

78. UK Met Office, How have cooling degree days (CDD) and heating degree days (HDD) been calculated in UKCP09? (2012). Accessed at http://ukclimateprojections.metoffice.gov.uk/22715 on 16 June 2014.

79. U.S. Energy Information Administration, Residential demand module of the National Energy Modeling System: Model documentation 2013, *Technical Report* (U.S. Energy Information Administration, 2013).

80. U.S. Energy Information Administration, Commercial demand module of the National Energy Modeling System: Model documentation 2013, *Technical Report* (U.S. Energy Information Administration, 2013).

81. US Energy Information Administration, Table F30: Total energy consumption, price, and expenditure estimates, 2012 (2014). Accessed at http://www.eia.gov/state/seds/data.cfm?incfile=/state/seds/sep_fuel/html/fuel_te.html&sid=US on 16 June 2014.

82. B. R. Jarvinen, C. J. Neumann, M. A. S. Davis, *NOAA Tech. Memo.* (1984). Available at http://www.nhc.noaa.gov/pdf/NWS-NHC-1988-22.pdf.

83. W. D. Collins *et al*., Description of the NCAR community atmosphere model (CAM 3.0), Technical Reports NCAR/TN-464+STR (National Center for Atmospheric Research, Boulder, CO, 2004).

84. G. A. Grell *et al*., A description of the fifth-generation Penn State/NCAR mesoscale model (MM5), Technical Reports NCAR/TN-398+STR (National Center for Atmospheric Research, Boulder, CO, 1994).

85. U.S. Bureau of Economic Analysis, GDP by industry / VA, GO, II, EMP (1997–2013, 69 industries) (2014). Accessed at http://www.bea.gov/industry/xls/GDPbyInd_VA_NAICS_1997-2013.xlsx on 8 August 2014.

86. U.S. Federal Bureau of Investigation, Crime in the United States, (2012).Accessed at www.fbi.gov/about-us/cjis/ucr/ucr-publications#Crime on 8 August 2014.

87. D. B. Diaz, Estimating global damages from sea level rise with the Coastal Impact and Adaptation Model (CIAM). *Clim. Change* **137**, 143–156 (2016). doi:10.1007/s10584-016-1675-4

88. U.S. Bureau of Economic Analysis, State GDP for all industries and regions (2008–2013) (2014). Accessed at https://goo.gl/2QGaEz on 8 August 2014.

89. G. Atkinson, S. Dietz, J. Helgeson, C. Hepburn, H. Saelen, Siblings, not triplets: Social preferences for risk, inequality and time in discounting climate change. *Economics: The Open-Access, Open-Assessment E-Journal* 3 (2009). http://www.economics-ejournal.org/economics/journalarticles/2009-26

90. U.S. Bureau of Economic Analysis, County personal income and population (Table CA1), 2008–2013 (2014). Accessed at https://goo.gl/p44pkw on 8 August 2014.

91. J. K. Anttila-Hughes, S. M. Hsiang, SSRN Working Paper 2220501 (2012). https://ssrn.com/abstract=2220501.